# A Detailed Theoretical Study of the Mechanism and Energetics of Methane to Methanol Conversion by Cisplatin and Catalytica

Ankan Paul and Charles B. Musgrave*

*Department of Chemical Engineering, Stanford University, 380 Roth Way, Stanford, California 94305*

*Received May 27, 2006*

The conversion of methane to methanol by dichloro($\eta^2$-{2,2′-bipyrimidyl})platinum(II) [Pt(Bpym)-$Cl_2$] (Catalytica) and $Pt(NH_3)_2Cl_2$ (cisplatin) [*Science* **1998**, *280*, 560] has been studied using hybrid density functional theory in conjunction with the conductor-like polarizable continuum solvent model (CPCM). We have determined the full potential energy profiles for plausible catalytic pathways along the three major phases of the catalytic cycle, namely, (a) C−H activation, (b) Pt(II) to Pt(IV) oxidation, and (c) functionalization. For Catalytica, oxidation of Pt(II) to Pt(IV) is the highest barrier step for all active catalytic forms considered. Oxidation of Pt(II) to Pt(IV) is significantly easier for cisplatin compared to Catalytica, explaining the faster catalytic transformation by cisplatin. Our calculations suggest that the oxidation barrier is significantly affected by the ligand environment on the Pt center of the catalyst. We predict that monoprotonation of the bipyrimidine ring of Catalytica significantly affects the oxidation process only if catalysis proceeds through electrophilic C−H activation *cis* to the protonated pyrimidine ring. We also determine a full potential energy profile for catalytic conversion by cisplatin proceeding through oxidative C−H addition, subsequent deprotonation, followed by oxidation of Pt(II) to Pt(IV), and then functionalization.

## Introduction

Although methane is an abundant natural gas and efficient fuel, its applications are limited by transportation and storage difficulties. Methanol, however, is more "mobile" and just as "clean", making it practical for many applications including use as an alternative energy source and in direct methanol fuel cells. Efficient transformation of methane to methanol is therefore important for practical and academic reasons as a sustainable, inexpensive catalytic process for this transformation that could significantly change the global fuel economy.

Few practical processes currently exist to accomplish this transformation. Effective procedures that pass methane gas over heterogeneous oxide catalysts at high temperatures have been studied since 1993.[1] Homogeneous methods[2−20] were first reported in the 1970s,[5,6] with the first notable route involving homogeneous transition-metal catalysts reported by Shilov, who discovered that square-planar Pt(II) complexes promote "C−H activation" of alkanes to form alkylated Pt(II) square-planar complexes. Methanol was obtained from methylated Pt(II) complexes using $K_2[PtCl_6]$, an expensive stochiometric outer-sphere oxidant. Periana and co-workers avoided the use of $K_2[PtCl_6]$ by carrying out "C−H activation" reactions with mercuric salts[10] and Pt(II) square-planar complexes[17] in fuming $H_2SO_4$, where the medium itself serves as an inner-sphere oxidant to produce methanol while it is itself reduced to $SO_2$. The cycle is sustained by aerially reoxidizing $SO_2$ to $SO_3$. Using the dichloro($\eta^2$-{2,2′-bipyrimidyl})platinum(II) [Pt(Bpym)$Cl_2$] (Catalytica) complex, they achieved catalytic transformation of methane to methanol in 70% one-pass yield and 80% selectivity at moderately high temperatures and pressures. The net chemical equation of the process is

$$CH_4 + 2H_2SO_4 = CH_3OSO_3H + H_2SO_3 + H_2O$$

Although cisplatin catalyzes this valuable transformation at a faster rate than Catalytica, it decomposes to form a polymer

* Corresponding author. E-mail: chasm@stanford.edu.

(1) (a) Hickman, D. A.; Schmidt, L. D. *Science* **1993**, *259*, 343. (b) For developments in this area see: *Oil Gas J.* **1997**, *95* (16), 16; U.S. Patents 4,833,170; 4,973,453; 4,686,238; 5,628,931; 5,658,497; 5,653,916; 5,639,401; 5,645,613; 5,621,155; 5,620,670; 5,543,437; 5,506,272; 5,504,118; 5,500,449; and 5,324,335.

(2) (a) Shilov, A. E.; Shul'pin, G. B. *Chem. Rev.* **1997**, *97*, 2879. (b) Stahl, S. S.; Labinger, J. A.; Bercaw, J. E. *Angew. Chem., Int. Ed.* **1998**, *37*, 2180. (c) Jones, W. D. *Science* **2000**, *287*, 1942. (d) Crabtree, R. H. *J. Chem. Soc., Dalton Trans.* **2001**. (e) Labinger, J. A.; Bercaw, J. E. *Nature* **2002**, *417*, 507. (f) Kakiuchi, F.; Murai, S. *Acc. Chem. Res.* **2002**, *35*, 826. (g) Ritleng, V.; Sirlin, C.; Pfeffer, M. *Chem. Rev.* **2002**, *102*, 1731. (h) Lersch, M.; Tilset, M. *Chem. Rev.* **2005**, *105*, 2471, and references therein.

(3) Shilov, A. E. *Activation of Saturated Hydrocarbons by Transition Metal Complexes*; D. Riedel Publishing Co.: Dordrecht, The Netherlands, 1984.

(4) Hill, C. L. *Activation and Functionalization of Alkanes*; Wiley-Interscience: New York, 1989.

(5) Gol_dshleger, N. F.; Tyabin, M. B.; Shilov, A. E.; Shteinman, A. A. *Zh. Fiz. Khim. (Engl. Transl.)* **1969**, *43*, 1222.

(6) Gol_dshleger, N. F.; Es_kova, V. V.; Shilov, A. E.; Shteinman, A. E. *Zh. Fiz. Khim. (Engl. Transl.)* **1972**, *46*, 785.

(7) Gretz, E.; Oliver, T. F.; Sen, A. *J. Am. Chem. Soc.* **1987**, *109*, 8109.

(8) Fujiwara, Y.; Jintoku, T.; Uchida, Y. *New J. Chem.* **1989**, *13*, 649.

(9) Kao, L.; Hutson, A. C.; Sen, A. *J. Am. Chem. Soc.* **1991**, *113*, 700.

(10) Periana, R. A.; Taube, D. J.; Evitt, E. R.; Loffler, D. G.; Wentrcek, P. R.; Voss, G.; Masuda, T. *Science* **1993**, *259*, 340.

(11) Lin, M; Sen, A. *Nature* **1994**, *368*, 613.

(12) Sen, A.; Benvenuto, M. A.; Lin, M; Hutson, A. C.; Basickes, N. *J. Am. Chem. Soc.* **1994**, *116*, 998.

(13) Lin, M.; Hogan, T. E.; Sen, A. *J. Am. Chem. Soc.* **1996**, *118*, 4574.

(14) Walktz, K. M.; Hartwig, J. F. *Science* **1997**, *277*, 211.

(15) Wick, D. D.; Goldberg, K. I. *J. Am. Chem. Soc.* **1997**, *119*, 10235.

(16) Holtcamp, M. W.; Labinger, J. A.; Bercaw, J. E. *J. Am. Chem. Soc.* **1997**, *119*, 848.

(17) Periana, R. A.; Taube, D. J.; Gamble, S.; Taube, H.; Satoh, T.; Fujii, H. *Science* **1998**, *280*, 560.

(18) Periana, R. A.; Mironov, O.; Taube, D.; Bhalla, G.; Jones, C. J. *Science* **2003**, *301*, 814.

(19) Böhm, V. P. W.; Weskamp, T.; Gstöttmayr, C. W. K.; Hermann, W. A. *Angew. Chem., Int. Ed.* **2000**, *39*, 1602.

(20) Siegbahn, P. E. M.; Crabtree, R. H. *J. Am. Chem. Soc.* **1996**, *118*, 4442.

10.1021/om060465j CCC: $37.00 
Publication on Web 01/10/2007

and ammonium sulfate in the sulfuric acid medium. Stability of the catalyst in concentrated $H_2SO_4$ is paramount for reasonable turnover. Periana et al. suggested that the [Pt(Bpym)$Cl_2$] complex is stable in concentrated $H_2SO_4$ because of Bpym's $\pi$-acid character and bidentate nature.[17]

Methane to methanol transformation employing "C−H activation" chemistry has inspired a number of theoretical investigations using density functional theory (DFT).[20−26] Hush et al. investigated the thermodynamics of the conversion of methane to methanol by cisplatin along with the activation barriers for C−H activation.[21,22] Ziegler et al. and Goddard et al. studied the thermodynamics and the kinetic barriers of C−H activation of methane by the Catalytica complex.[23,24] These studies revealed valuable insights, but also produced some conflicting results. For example, Hush and co-workers suggested that for cisplatin $CH_4$ displaces $NH_3$ from the complex to form the $\sigma$-complex,[22] whereas Goddard et al. asserted that methane displaces a chloride from cisplatin in forming the $\sigma$-complex.[25]

Goddard and co-workers also carried out extensive studies to investigate the stabilities of the Catalytica and cisplatin complexes.[25,26] Their hybrid DFT-based thermodynamic studies employed the Poisson−Boltzmann solvation model and indicated that the Bpym ligand is protonated in concentrated $H_2SO_4$.[25,26] Moreover, they suggested that the availability of extra protonation sites on Bpym other than the N-donor sites attached to the Pt center confers stability to the complex.[25,26] However, their thermodynamic calculations predict that protonation is unfavorable for the rate-determining Pt(II) to Pt(IV) oxidation step. Ziegler and co-workers using a pure DFT functional with the COSMO solvent model predicted that the Bpym ligand of Catalytica does not undergo protonation in concentrated $H_2SO_4$.[23,24] These conflicting conclusions regarding protonation leave unanswered the questions of the importance of protonation in dictating the stability of the catalyst in concentrated $H_2SO_4$ and whether protonation has a significant effect on the key activation barriers involved in the catalytic process.

The catalytic cycles of Catalytica and cisplatin involve three major stages: (a) C−H activation to form the methylated Pt(II) complex, (b) oxidation of the methylated Pt(II) complex to form a Pt(IV) complex, and (c) functionalization of the methyl group to form $CH_3OSO_3H$ through $S_N2$ nucleophilic attack on the methyl by a bisulfate anion. Periana et al. employed isotopic exchange for the Catalytica system to convincingly establish that Pt(II) to Pt(IV) oxidation is the rate-determining step.[17] Although the associated C−H activation barriers for Catalytica have been theoretically investigated by both Ziegler and Goddard, the oxidation step has received much less attention.[23−26]

Ziegler et al. used a linear transit scan, a constrained search algorithm, to study the reaction mechanism and locate the transition states associated with the oxidation process of Catalytica.[24] They suggested that $SO_3$ oxidizes the methylated Pt(II) center to Pt(IV) and then the methyl group is functionalized via $S_N2$ attack by $HSO_4^-$.[24] Although this work contributed considerably to the understanding of the post C−H activation phases of the catalytic cycle, it did not theoretically establish oxidation as the rate-determining step. Furthermore, the effect of protonation on the oxidation step was not examined.

No theoretical study to date has shown the oxidation step to be rate determining, nor has a full potential energy profile for the catalytic process of methane to methanol transformation by Catalytica been reported. Although it has been suggested that the catalytic cycle may involve oxidative C−H addition,[23,24] no mechanism with computed barriers connecting the oxidative addition C−H mode with the following reaction phases of the catalytic cycle has been reported. Similarly, for cisplatin limited studies have implicated the oxidative addition mode of C−H activation as a likely pathway for the catalytic cycle, but no barriers have been yet reported for the subsequent oxidation and functionalization steps.

The barrier for Pt(II) to Pt(IV) oxidation is sensitive to the ligand environment on the Pt center and may determine the overall rate of methane to methanol conversion by different Pt complexes. The fact that cisplatin, despite being unstable, converts methane to methanol faster than Catalytica suggests that oxidation is significantly faster in the case of cisplatin than Catalytica. This suggests that better catalysts might be designed with the stability of Catalytica and the catalytic ability of cisplatin or possibly with desirable attributes exceeding those of either of these complexes. The rational design of improved catalysts depends on the elucidation of what molecular features influence a complex's catalytic ability and on a fundamental understanding of the catalytic process, its full mechanism, and associated potential energy profiles. We anticipate that a detailed theoretical description of the intermediates and transition states of methane to methanol conversion by these two catalysts will add to a conceptual framework to support the rational exploitation of ligand effects to develop better methane to methanol catalysts.

Here, we use B3LYP DFT in conjunction with the CPCM (COSMO) solvent model[27,28] to explicitly carry out a comparative study of the catalytic pathways involved in the transformation of methane to methanol by cisplatin and Pt[Bpym]$Cl_2$ in concentrated $H_2SO_4$. Our main objectives are to (a) determine the full catalytic pathways for Catalytica, cisplatin, and associated species, including the identification of intermediates and transition states, (b) resolve what affects the catalytic abilities of cisplatin, Catalytica, and related species by comparing the relative energies of their key transitions states and intermediates, (c) clarify the effect of protonation on the critical activation barriers of the catalytic cycle for Catalytica, and particularly the oxidation barrier, and (d) establish whether the cisplatin catalytic cycle operates through oxidative C−H addition or via electrophilic C−H activation.

## Computational Details

All quantum chemical calculations have been carried out using the Gaussian 03 suite of programs.[29] We have used B3LYP, which employs the Becke3 gradient-corrected hybrid exchange functional, as implemented in Gaussian 03[30] for optimizing all the molecular structures of relevant intermediates and transition states. Pt is described with the Los Alamos double-$\zeta$ basis set along with the corresponding Pt pseudopotential (LANL2DZ).[31−33] All other atoms

(21) Mylavaganam, K.; Backsay, G. B.; Hush, N. S. *J. Am. Chem. Soc.* **1999**, *121*, 4633.
(22) Mylvaganam, K.; Bacskay, G. B.; Hush, N. S. *J. Am. Chem. Soc.* **2000**, *122*, 2041.
(23) Gilbert, T. M.; Hristov, I.; Ziegler, T. *Organometallics* **2001**, *20*, 1183.
(24) Hristov, I. H.; Ziegler, T. *Organometallics* **2003**, *22*, 1668.
(25) Kua, J.; Xu, X.; Periana, R. A.; Goddard, W. A. *Organometallics* **2002**, *21*, 511.
(26) Xu, X.; Kua, J.; Periana, R. A.; Goddard, W. A. *Organometallics* **2003**, *22*, 2057.
(27) Barone, V.; Cossi, M. *J. Phys. Chem. A* **1998**, *102*, 1995.
(28) Cossi M.; Rega, N.; Scalmani, G.; Barone, V. *J. Comput. Chem.* **2003**, *24*, 669.
(29) Frisch, M. J.; et al. *Gaussian 03*, revision C.02; Gaussian, Inc.: Wallingford, CT, 2004.
(30) Stephens, P. J.; Devlin, F. J.; Chabalowski, C. F.; Frisch, M. *J. Phys. Chem.* **1994**, *98*, 11623.
(31) Hay, P. J.; Wadt W. R. *J. Chem. Phys.* **1985**, *82*, 270.

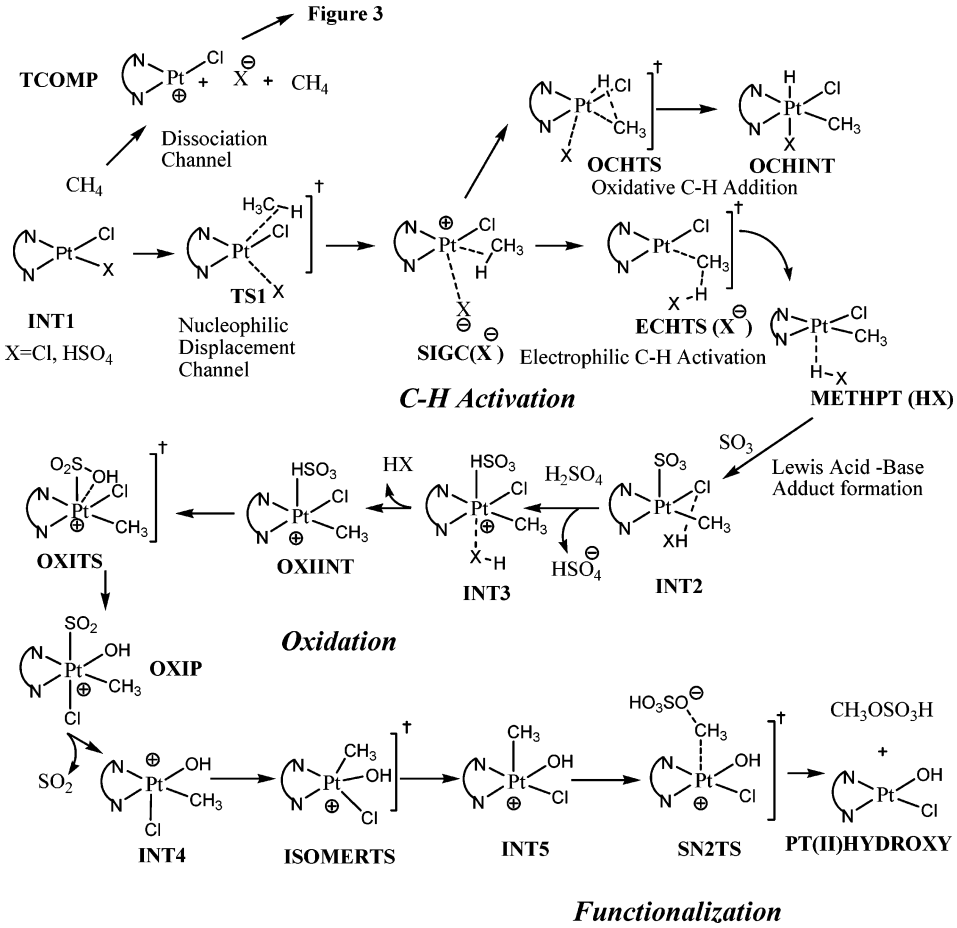


**Figure 1.** Schematic representation of the catalytic route for methane to methanol conversion by the Pt(II) catalysts Catalytica and cisplatin.

are described using the 6-31G+(d,p) basis set, which includes polarization functions for heavy atoms and hydrogens and a set of diffuse functions for all heavy atoms. All molecular structures were fully optimized with harmonic frequencies computed in the "gas phase". A fine grid with 75 radial and 320 angular points was employed for numerical integration. All intermediates were characterized by the absence of imaginary frequencies. Transition states were confirmed by computing the gas phase Hessian analytically and confirming the presence of a single negative eigenvalue (single imaginary frequency). IRC (intrinsic reaction coordinate) computations were carried out for key transition states (related to the catalytic cycle of cisplatin) to check if they connect the desired minima. For the solvent phase calculations, single-point energies were calculated for the gas-phase-optimized structures with the CPCM solvent model as implemented in Gaussian 03. Previous investigations have used similar methodologies with satisfactory results.[34] The CPCM solvent parameters were selected for 98% $H_2SO_4$ with a dielectric constant of 98.0, a solvent probe radius of 2.205 Å,[25] and a solvent density of 0.011 molecule/Å$^3$. For the solute atomic radii we have used the atomic radii from the universal force field. The total energies from solvent computations were corrected for zero-point effects by adding the zero-point energies obtained from the calculated gas phase frequencies. All relative energies reported in the Results and Discussion section are relative energies in solution phase with zero-point energies unless stated otherwise. The energies of intermediates and transition states along with the byproducts are indicated relative to **INT1**, the starting complex, and the reagents ($SO_3$ and $H_2SO_4$, and $Cl^-$ for some pathways) for each individual catalytic cycle unless stated otherwise. Note that to simplify figures potential energy diagrams sometimes do not show all reagents and byproducts, although they contribute to the computed relative energy. All balanced equations are provided in the Supporting Information.

(32) Hay, P. J.; Wadt W. R. *J. Chem. Phys.* **1985**, *82*, 284.
(33) Hay, P. J.; Wadt W. R. *J. Chem. Phys.* **1985**, *82*, 299.
(34) Shahji, C.; Bell, A. T. *J. Am. Chem. Soc.* **2006**, *127*, 2041.

## Results and Discussions

Figure 1 illustrates a schematic description of the intermediates and transition states for the (a) C−H activation, (b) oxidation of Pt(II) to Pt(IV), and (c) functionalization to form $CH_3SO_3H$ stages of the full catalytic cycle.

Figure 2 shows complexes considered for the Catalytica (**1** to **4**) and cisplatin (**5** and **6**) catalyzed reactions. The specific species considered are (**1**) Pt(Bypm)$Cl_2$, also called Catalytica; (**2**) Pt(Bypm)Cl($HSO_4$), a mixed chloro-bisulfate Pt(II) complex formed from **1** through ligand exchange with the medium; (**3**) [Pt(BpymH)$Cl_2$]$^+$, with the protonated backbone of the Bpym ligand of complex **1**; and (**4**) [Pt(BypmH)Cl($HSO_4$)]$^+$, the protonated form of **2**; and for cisplatin (**5**) $(NH_3)_2PtCl_2$, also called cisplatin; and (**6**) $(NH_3)_2$PtCl($HSO_4$), the cisplatin analogue of **2** formed through ligand exchange. Catalytic complexes **2**, **3**, and **4** for Catalytica were considered in previous computational studies by Goddard et al.,[25] who suggested their possible roles as active catalysts. Similar considerations have led us to examine catalytic cycles for both **5** and **6**. Reaction of cisplatin with $H_2SO_4$ from the medium can yield other active forms formed through exchange of $NH_3$ with sulfuric acid. However, in this study we restrict ourselves to an examination of the starting forms that retain the N-sp$^3$ donors. Additionally, we have examined the effect of varying the electronic nature of the N-donor ligands to the Pt(II) center on the oxidation of Pt(II) to Pt(IV).

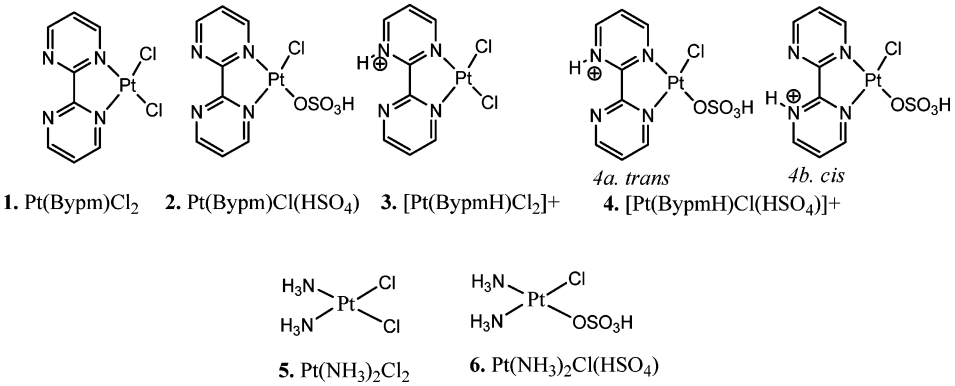


**Figure 2.** Molecular species that are plausible candidates for carrying out oxidation of methane to methanol catalytically in concentrated $H_2SO_4$ for Catalytica (**1**, **2**, **3**, and **4**) and cisplatin (**5** and **6**).

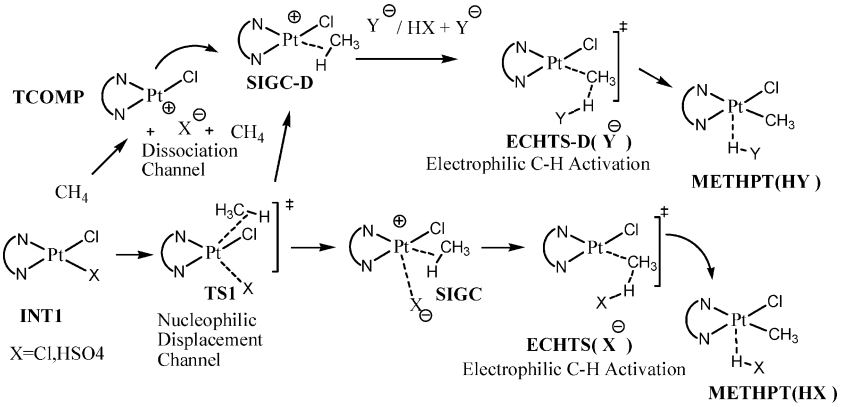


**Figure 3.** Schematic route of C−H activation of complex **1** initiating through dissociation and nucleophilic displacement channels.

**A. $\sigma$-Complex Formation and C−H Activaton.** It is reasonable to assume that $CH_4$ displaces a chloride ligand from the Pt(II) center of the Catalytica complex, rather than a N donor of the bidentate Bpym ligand considering the related entropic factors. This results in the $\sigma$-complex **SIGC**($X^-$) or $\sigma$-complex **SIGC-D** (which has the counterion $X^-$ dissociated from $\sigma$-complex **SIGC**($X^-$); see Figure 3), where the C−H $\sigma$-bond of methane acts as a donor to the Pt(II) center. Two modes through which $\sigma$-complex formation can occur are plausible: (a) dissociation of the chloride ligand and subsequent formation of the $\sigma$-complex by association with methane and (b) direct displacement (nucleophilic displacement) (see Figure 3) of the chloride ligand from the Pt(II) center by methane. Our gas phase calculations indicate that mode (b) is favored over mode (a) by 10.0 kcal/mol for complex **1**. However, the trend is reversed in solution, where the dissociative pathway is favored over nucleophilic displacement by 7.7 kcal/mol! Figure 3 illustrates a schematic description of these two pathways leading to C−H activation through the electrophilic C−H activation pathway.

The energy cost for dissociating $Cl^-$ from complex **1** is 30.1 kcal/mol, while dissociating $HSO_4^-$ from complex **2** requires only 19.8 kcal/mol. Similar energetic penalties are predicted for the protonated analogues, where **TCOMP** lies 28.9 and 15.2 kcal/mol above **INT1**, the initial complex formed between the Pt(II) complex and methane, for complexes **3** (see Figure 4 for optimized molecular geometries) and **4**, respectively. We find that the nucleophilic displacement barrier (**TS1**) to displace $Cl^-$ by methane is significantly higher, with **TS1** 37.8 kcal/mol above **INT1**. Our gas phase calculations indicate that the transition state for the direct displacement channel (b) lies 2.0 kcal/mol above **SIGC**($Cl^-$) for complex **1**. However, for **1** in sulfuric acid the situation reverses, with **SIGC**($Cl^-$) higher in energy than **TS1** by 2.4 kcal/mol. We also find that **SIGC**($Cl^-$)

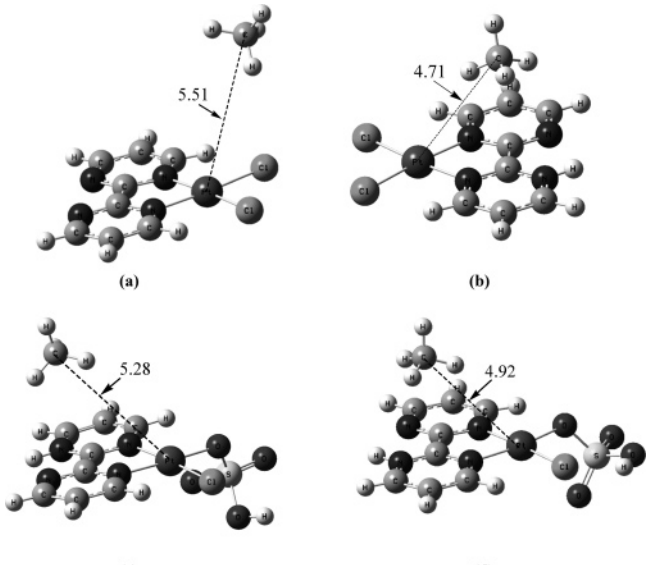


**Figure 4.** Optimized molecular structures of (a) **INT1** for complex **1**, (b) **INT1** for complex **3**, (c) **INT1-4a** for complex **4** (*trans* isomer), and (d) **INT1-4b** for complex **4** (*cis* isomer). All bond lengths are in angstroms.

is 42.2 kcal/mol higher in energy than **INT1**, whereas **TS1** lies 37.8 kcal/mol above **INT1**. To determine the origin of the effect of solvation on the relative energies considered, the calculated dipole moments for various species were examined. Our predicted dipole moment for **SIGC**($Cl^-$) ($\mu$ = 8.45 D) is smaller that of **TS1** ($\mu$ = 9.99 D), indicating a larger stabilization of **TS1** with respect to **INT1** in the highly polar medium. The predicted relative energies of **SIGC**($Cl^-$) with respect to **INT1**

are significantly different from the earlier results of Goddard et al.,[25] who predicted that **SIGC**($Cl^-$) lies only 28 kcal/mol above **INT1**.[25] In their calculations they employed the Poisson−Boltzmann solvent model to compute single-point energies at gas phase B3LYP/LACVP**(+)-optimized structures. It is surprising that using a slightly different basis set and the CPCM solvent model results in a 14.0 kcal/mol difference. On the other hand, they predict **TS1** to be 40.0 kcal/mol at 0 K, which is in good agreement with our result of 37.8 kcal/mol. In contrast, we predict that the displacement of $HSO_4^-$, a better leaving group than $Cl^-$, by methane from complex **2** is 29.6 kcal/mol.

The two different pathways (Figure 3) for ligand exchange lead to the formation of the **SIGC**($X^-$) and **SIGC-D** intermediates. **SIGC**($X^-$) differs from **SIGC-D** in that **SIGC** has the counterion $X^-$ loosely bound to the metal center, where $X^-$ is either $Cl^-$ or $HSO_4^-$. In the highly polar solvent phase the counterion $X^-$ can dissociate from **SIGC**($X^-$) to form **SIGC-D** and free $X^-$. For **1**, dissociation of $Cl^-$ from **SIGC**($Cl^-$) to form **SIGC-D** is exothermic by 12.0 kcal/mol due to the significant stabilization of the separated and solvated ions in the highly polar medium, suggesting that **SIGC**($Cl^-$) is not formed in solution phase and that for **1** the more likely intermediate en route to C−H activation is **SIGC-D**. For all $\sigma$-complexes pertaining to the Bpym and protonated Bpym Pt(II) catalytic species we find that dissociation of counterion $X^-$ from **SIGC**($X^-$) is favored, leading to the formation of SIGC-D and $X^-$. This suggests that the nucleophilic displacement pathway through **TS1** leads to the formation of the **SIGC-D** intermediate rather than the **SIGC**($X^-$) intermediate in the highly polar concentrated sulfuric acid medium. As a result, we consider **SIGC-D** as the intermediate en route to C−H activation for both the nucleophilic and the dissociative pathways for complexes **1** to **4**.

Monoprotonation of the Bpym backbone of Catalytica introduces several possibilities. We find that monoprotonation of Bpym on **1** is favored by 1.6 kcal/mol at 0 K. Given the excess number of $H_2SO_4$ molecules in concentrated $H_2SO_4$, it is reasonable to assume that all active catalytic forms and intermediates of Catalytica will be monoprotonated. Diprotonation is significantly unfavorable, as has been indicated previously by both Goddard and Ziegler.[24,25] Diprotonation of **1** is unfavorable by 15.9 kcal/mol according to our computations.

Monoprotonation of **2** leads to the two isomers **4a** and **4b**, giving rise to two possible isomers of **INT1** (see Figure 4) for complex **4**, where *trans*-**INT1** with bisulfate *trans* to the protonated ring is slightly more stable (by 3.1 kcal/mol) than *cis*-**INT1** (bisulfate ligand *cis* to the protonated ring). The dissociation of $HSO_4^-$ from both **4a** and **4b** led to identical **TCOMP** species, and hence the same intermediates and transition states are encountered for both isomers along the reaction path. To compute the reaction barriers for complex **4**, we take into consideration only **INT1-4a**.

The dissociative pathway to **SIGC-D** formation is favored over the nucleophilic displacement pathway for complex **3**. Dissociating $Cl^-$ requires 29.2 kcal/mol from **INT1**, whereas **TS1** (see Figure 5) for the nucleophilic displacement (with $CH_4$ approaching *trans* to the protonated pyrimidine ring) pathway lies 40.7 kcal/mol above **INT1** for complex **3**. Furthermore, **TS1** for the corresponding *cis* nucleophilic displacement (see Figure 5) lies 46.8 kcal/mol above **INT1**. For complex **4** only the dissociative pathway was investigated. Dissociating $HSO_4^-$ from **4** requires 15.2 kcal/mol. Intriguingly, the optimized structure of **TCOMP** formed from dissociating $Cl^-$ from **3** or $HSO_4^-$ from **4** shows that the $Cl^-$ ligand prefers a *cis* orientation to the nonprotonated pyrimidine ring. We calculate a low-frequency vibrational mode of 46 $cm^{-1}$, corresponding to a floppy wagging mode of the Pt−Cl bond between the positions *cis* and *trans* to the unprotonated ring. We did not locate an analogous *trans* minimum, as all our guess geometries for this structure collapsed to the **TCOMP** geometry, where the Cl is *cis* to the protonated ring. **TCOMP** (see Figure 6) can form **SIGC-D-3a** or **SIGC-D-3b** (Figure 6) on the basis of the mode of approach of the methane molecule. The floppy Pt−Cl bond wagging mode suggests that possibly both the protonated *cis* and *trans* isomers of **SIGC-D** can be formed. Interconversion between the *cis*−*trans* monoprotonated forms is likely through a low barrier proton shuttling mechanism by $HSO_4^-$, most likely hydrogen bonded to Bpym, as shown in Figure 7.

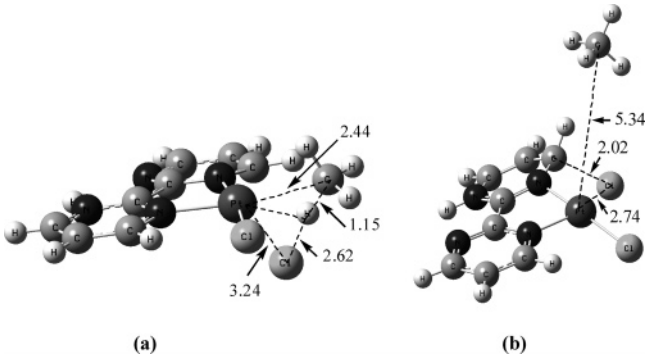


**Figure 5.** Optimized molecular structures of **TS1** for complex **3** with methane approaching the Pt center (a) *trans*, **TS1-3a**, and (b) *cis*, **TS1-3b**, to the protonated pyrimidine ring for complex **3**. All bond lengths are in angstroms.

All subsequent discussions pertaining to protonated complexes involve only monoprotonated forms. The Bpym ligand has two N atoms within each six-membered aromatic ring that are highly electron deficient. One nitrogen atom of each pyrimidine ring acts as a $\sigma$-donor to the Pt center and makes the ring in turn more electron deficient. Moreover, protonation can further reduce the electron density on the rings, making them susceptible to nucleophilic attack. Methane can displace the chloride *cis* or *trans* to the protonated pyrimidine ring. Gas phase optimizations led to structures for transition states and corresponding $\sigma$-complexes that showed the displaced $Cl^-$ interacting with the ring carbon adjacent to the N-donor to the Pt center. This feature is more pronounced for the pathway involving displacement of $Cl^-$ *cis* to the ring and can be identified further by the puckering of the pyrimidine ring (see Figures 5 and 8). For both the *cis* and *trans* displacement pathways we found that the **SIGC**($Cl^-$) complexes are significantly higher in energy compared to the corresponding transition states (**TS1**) (10 and 12 kcal/mol) in solution phase. This suggests that in solution phase the interaction between the pyrimidine ring and the displaced $Cl^-$ is highly unfavorable and if the nucleophilic displacement pathways are operative, they will form **SIGC-D** intermediates with the displaced $Cl^-$ having no interaction with the complex moieties, with the enhanced solvation of the oppositely charged ions driving the dissociation.

Unlike Catalytica, which has the Bpym bidentate N-donor ligand that cannot be displaced by a weak ligand like $CH_4$ due to entropic factors, in cisplatin alternative catalytic routes through dissociation of monodentate $NH_3$ ligands can exist. We find the energetic penalty incurred in dissociating $NH_3$ from cisplatin (22.1 kcal/mol) is larger compared to that for dissociating $Cl^-$ from cisplatin (12.2 kcal/mol). However, the energy required for dissociating $NH_3$ from cisplatin is not so prohibitively high as to eliminate a catalytic cycle originating through this route. Because this path deviates from the focus

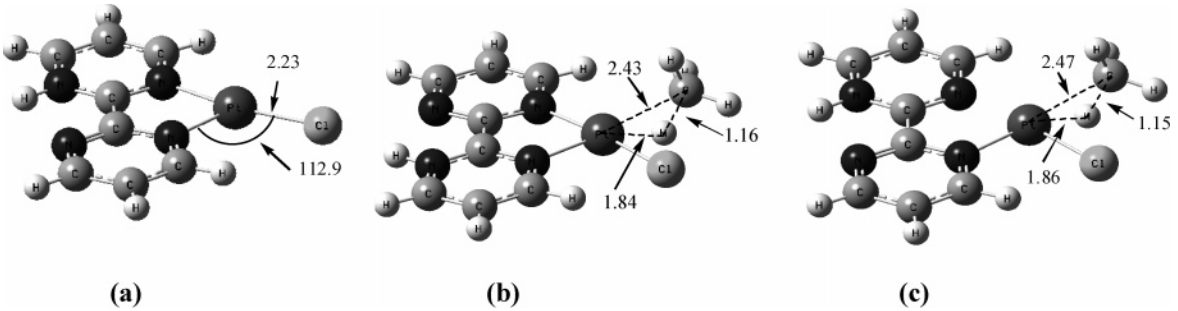


**Figure 6.** Optimized molecular structures for (a) **TCOMP**, (b) **SIGC-D-3a**, and (c) **SIGC-D-3b** for complex **3**. All bond lengths are in angstroms and angles are in degrees.

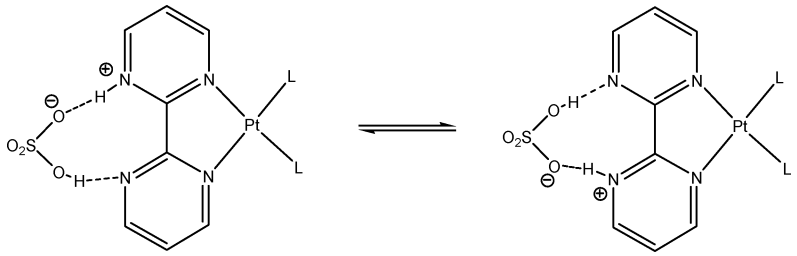

**Figure 7.** Schematic diagram of proton shuttling through a hydrogen-bonded $HSO_4^-$ anion.

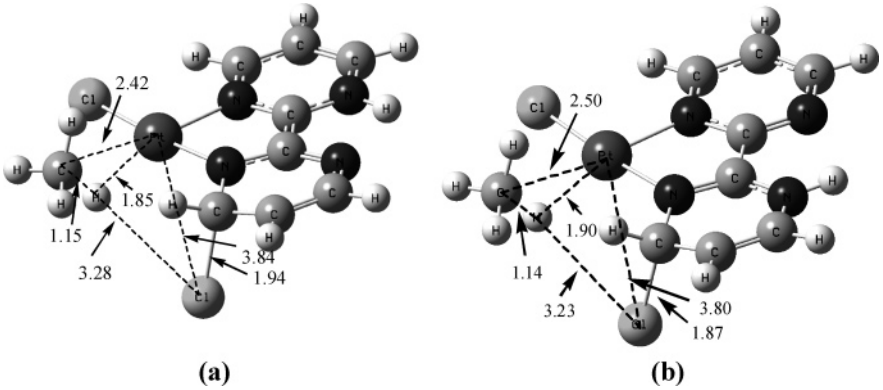


**Figure 8.** Optimized molecular structures of **SIGC**($Cl^-$) for complex **3** with methane approaching the Pt center (a) *trans*, **SIGC**($Cl^-$)**-3a**, and (b) *cis*, **SIGC**($Cl^-$)**-3b**, to the protonated pyrimidine ring for complex **3**. All bond lengths are in angstroms.

of this report on investigating the influence of changing the type of N-donors ligated to the Pt center on activation barriers, we restrict our choices to catalytic pathways where the N-donors are retained throughout the catalytic cycle. However, the catalytic process originating from loss of $NH_3$ is currently under investigation.

In the case of cisplatin (**5**) we observe that displacing $Cl^-$ is significantly easier than for Catalytica (**1**). This is expected because the $sp^3$-N center of $NH_3$ is a better $\sigma$-donor than the more electronegative $sp^2$-N center of Bypm and hence significantly weakens the Pt−Cl bond *trans* to it. This effect is also observed for dissociation energies of $Cl^-$ and $HSO_4^-$ in cisplatin. Furthermore, the gas-phase-optimized transition state for $Cl^-$ displacement from cisplatin (**TS1**) (see Figure 9) shows a hydrogen-bond-like interaction between the leaving $Cl^-$ and the H attached to the $NH_3$ ligands. This likely decreases the $Cl^-$ displacement barrier relative to that of the analogous Catalytica complex (**1**). Not surprisingly, we observe that the barrier to displacement of $HSO_4^-$ from $(NH_3)_2PtCl(HSO_4)$ (**6**) by methane is 26.2 kcal/mol, 4.2 kcal/mol lower than that of the Pt(Bypm)-$Cl(HSO_4)$ complex.

C−H activation follows $\sigma$-complex formation. It has been suggested that two significant routes for C−H activation exist: (a) electrophilic C−H activation and (b) oxidative C−H

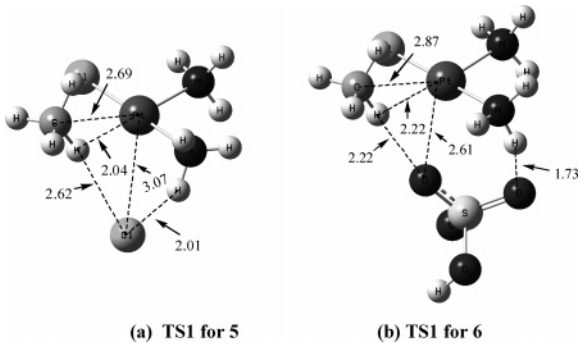


**Figure 9.** Optimized molecular structures of **TS1** (a) for complex **5** and (b) for complex **6**. All bond lengths are in angstroms.

addition.[14,15] Electrophilic C−H activation requires that the leaving or dissociated ligand, or an external base (anion), captures the acidic hydrogen from the activated C−H bond, leading to the formation of the Pt(II)-$CH_3$-methylated complex, **METHPT**(HX), whereas oxidative addition leads to the formation of a Pt(IV) hydrido methyl complex (**OCHINT**). The optimized molecular structures of transition states corresponding to electrophilic C−H activation for the protonated Catalytica complexes **3** and **4** are shown in Figure 10.

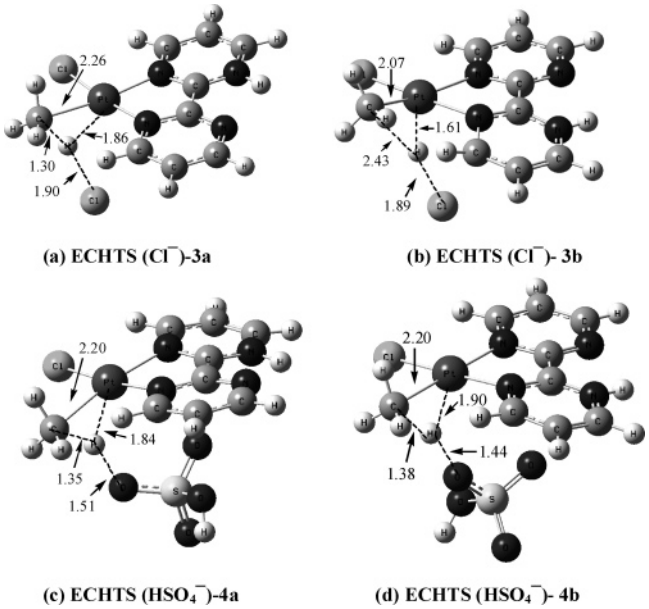


**Figure 10.** Optimized molecular geometries of transition states for electrophilic C−H substitution for complexes **3** and **4** (protonated Catalytica species). C−H activation by $Cl^-$ and $HSO_4^-$ *trans* (a and c) and *cis* (b and d) to the protonated pyrimidine ring. All bond lengths are in angstroms.

For Pt[Bpym]$Cl_2$ (**1**) the non-zero-point-corrected activation barrier to electrophilic C−H activation through electrophilic C−H substitution, the energy of **ECHTS**($Cl^-$) relative to **SIGC**($Cl^-$), is 2.2 kcal/mol in the gas phase. The reaction becomes barrierless in solution, in contrast to the 11.5 kcal/mol barrier predicted previously.[25] This also holds true for the protonated catalyst. The difference arises from the predicted energetics of **SIGC**($Cl^-$) relative to **INT1** for **1** and **3**. Our predicted energetics differ significantly from those reported previously.[25] However, **ECHTS**($Cl^-$), where the anion in parentheses facilitates the C−H activation, lies 11.5 kcal/mol above **SIGC-D** for **1** (see Figure 11). The lowest barrier for electrophilic C−H activation by $Cl^-$ for complex **3** is 10.6 kcal/mol (energy of **ECHTS**($Cl^-$) relative to **SIGC-D** for C−H activation occurring *trans* to the protonated ring; see Figure 13). The barrier to oxidative addition is higher than the barrier to electrophilic addition for complexes **1**, **2**, **3**, and **4**, in agreement with the results of Goddard et al. for complex **1**.[25] The potential energy profiles for C−H activation by complexes **1**−**4** are shown in Figures 11−14.

Along the dissociative pathway, electrophilic C−H activation is likely to be carried out either by the dissociated $Cl^-$ or by $HSO_4^-$ formed from the protonation of $Cl^-$ (as shown in Figure 3). Because $Cl^-$ is a stronger base than $HSO_4^-$, we observe that the electrophilic C−H activation barrier (energy **of ECHTS-D**($X^-$) relative to **SIGC-D**) is higher when the proton is abstracted by $HSO_4^-$ than by $Cl^-$ (a difference of 2.0 kcal/mol for **1**) for all the cases studied herein. A schematic representation of the PESs corresponding to these pathways is shown in Figure 11 for **1**. For the dissociative pathway involving **2** an analogous mechanism can occur (Figure 12). We notice that **ECHTS-D**($HSO_4^-$) lies 35.3 kcal/mol above **INT1** for **2**, whereas **ECHTS-D**($Cl^-$) lies 33.1 kcal/mol above **INT1**. Although the pathway for C−H activation involving $Cl^-$ has the lowest maximum barrier for complex **2**, this may not be the major channel for C−H activation, as free $Cl^-$ is likely to be present in low concentration in concentrated $H_2SO_4$ due to protonation. However, Periana et al. have observed trace amounts of $CH_3Cl$ in the reaction medium, suggesting the possibility that free chloride has led to the functionalization of methane.[17] Hence, C−H activation by $Cl^-$ cannot be ruled out for complexes **2** and **4**. For **3** we again find that the dissociative pathway is significantly favored over nucleophilic displacement (Figure 13). The lowest activation barrier to C−H activation for **3** is 40.0 kcal/mol along the **ECHTS-D**($Cl^-$) pathway. Figure 14 shows the dissociative pathways leading to C−H activation for complex **4**, where the pathway with the lowest barrier to C−H activation occurs via **ECHTS-D**($Cl^-$) with an energy 30.0 kcal/mol above **INT1** (Figure 14).

In the case of cisplatin the barriers associated with C−H activation are notably different. The 12.4 kcal/mol transition state energy of **ECHTS**($Cl^-$) relative to **SIGC**($Cl^-$) for **5** is substantially larger than for **1**, where **ECHTS**($Cl^-$) lies below **SIGC**($Cl^-$). The higher barrier for **5** arises because $Cl^-$ becomes a weaker base, as it has a hydrogen-bond-like interaction with the acidic hydrogen of the $NH_3$ ligand bound to the Pt(II) center in the transition state (see Figure 15) when it is capturing the proton of the C−H bond coordinated to the Pt(II) center. However, **ECHTS**($Cl^-$) is lower in energy (relative to **INT1**) for **5** (36.4 kcal/mol) than for **1** (40.4 kcal/mol), suggesting that C−H activation is considerably easier with cisplatin (**5**) than with Catalytica (**1**) via this route. This trend is contrary to previously reported barriers.[25]

For cisplatin we predict that oxidative addition is favored over electrophilic C−H activation by only 2.2 kcal/mol, whereas it was previously reported as being favored by 10.1 kcal/mol[25] (for PESs for **5** and **6** see Figures 16 and 17). We discuss the probable existence of a catalytic route through oxidative C−H addition after section C, which discusses functionalization.

**B. Oxidation of Pt(II) to Pt(IV).** Periana and co-workers suggested that oxidation proceeds through reaction of the Pt(II) methylated intermediate with $SO_3$, the acid anhydride of sulfuric acid.[24] The catalytic cycle is sustained by passing $SO_3$, which oxidizes Pt(II) to Pt(IV) and is itself reduced to $SO_2$, through the reaction media. Along the same lines Ziegler et al. investigated the oxidation step employing $SO_3$ as the oxidant and located relevant transition states using constrained optimization schemes.[24] Goddard et al. have suggested pathways for Pt(II) to Pt(IV) oxidation that proceed via a proton shuttling mechanism involving an $H_2SO_4$ molecule interacting with Bpym.[25] This mechanism is thus specific to protonated Catalytica complexes (**3** and **4**) because it can be applied only to complexes with ligands that can be protonated on the ligand backbone. Unfortunately, no transition states along this pathway have yet been reported.[25] Our repeated attempts to locate pathways for oxidation with $H_2SO_4$ failed to yield any meaningful results. The oxidation mechanism suggested by Ziegler et al. involving $SO_3$[24] can generally be applied to different kinds of ligand environments on Pt(II). We assume that the general mechanism of oxidation in concentrated $H_2SO_4$ is likely to be independent of the ligand environment, and hence the mechanism suggested by Ziegler et al. is a highly probable pathway for this route.

$SO_3$ is usually believed to be the oxidant in concentrated $H_2SO_4$, and Periana has demonstrated that the catalytic process is sustained by passing $SO_3$ through the reaction medium.[24] Consequently, it is expected that $SO_3$ is the oxidizing agent for conversion of Pt(II) to Pt(IV).[24] In contrast, a possible mechanism suggested by Goddard and co-workers does not involve $SO_3$ as an oxidant, but involves $H_2SO_4$.[24] Our results show that Pt(II) centers of methylated Pt(II) intermediates (**METHPT**(HX)) have a filled $5d_{z^2}$ HOMO. This fact led us to believe that

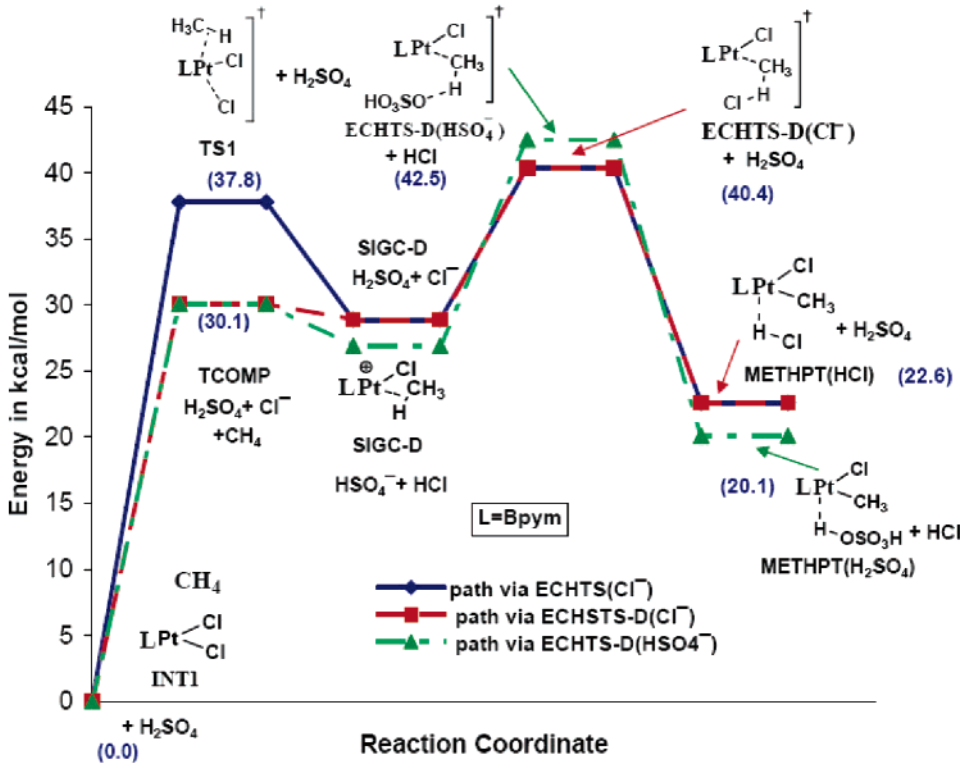


**Figure 11.** C−H activation by complex **1** through electrophilic substitution pathways: (1) nucleophilic displacement via **ECHTS**($Cl^-$) to form the $\sigma$-complex and subsequent electrophilic C−H activation by $Cl^-$, (2) dissociation of $Cl^-$ via **ECHTS-D**($Cl^-$) to form the $\sigma$-complex and subsequent electrophilic C−H activation by $Cl^-$, and (3) dissociation of $Cl^-$ via **ECHTS-D**($HSO_4^-$) to form the $\sigma$-complex and subsequent electrophilic C−H activation by $HSO_4^-$. Energies relative to **INT1** for key transition states and intermediates are shown in parentheses.

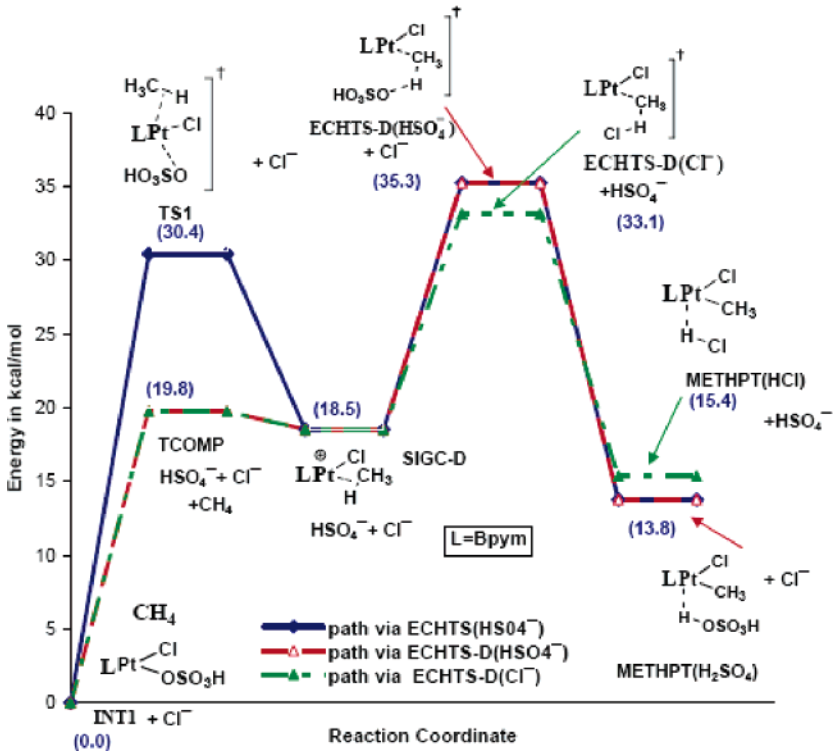


**Figure 12.** C−H activation by complex **2** through electrophilic substitution pathways: (1) nucleophilic displacement to form the $\sigma$-complex via **ECHTS**($HSO_4^-$) and subsequent electrophilic C−H activation by $HSO_4^-$, (2) dissociation of $HSO_4^-$ to form the $\sigma$-complex via **ECHTS-D**($HSO_4^-$) and subsequent electrophilic C−H activation by $HSO_4^-$, and (3) dissociation of $HSO_4^-$ to form the $\sigma$-complex via **ECHTS-D**($Cl^-$) and subsequent electrophilic C−H activation by $Cl^-$. Energies relative to **INT1** for key transition states and intermediates are shown in parentheses.

oxidation occurs through removal of electrons from the $5d_{z^2}$ orbital of Pt(II). Because **METHPT**(HX) intermediates are nucleophilic in nature, oxidation proceeds through Lewis acid−base type interactions with $SO_3$, as indicated by Ziegler et al.[24]

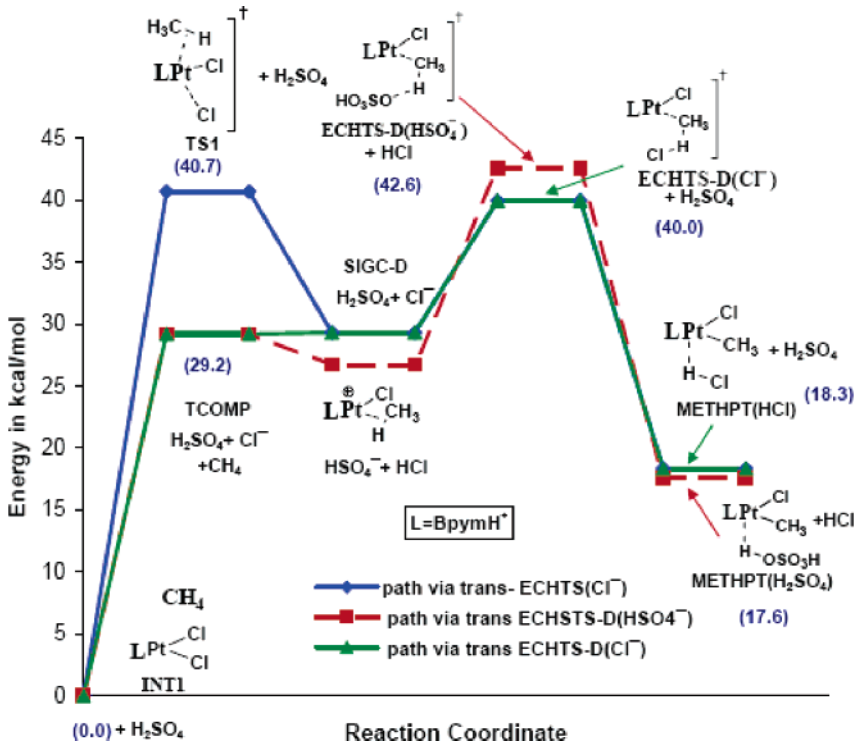


**Figure 13.** C−H activation by complex **3** through electrophilic substitution pathways: (1) nucleophilic displacement to form the $\sigma$-complex via **ECHTS**($Cl^-$) and subsequent electrophilic C−H activation by $Cl^-$, (2) dissociation of $Cl^-$ to form the $\sigma$-complex via **ECHTS-D**($Cl^-$) and subsequent electrophilic C−H activation by $Cl^-$, and (3) dissociation of $Cl^-$ to form the $\sigma$-complex via **ECHTS-D**($HSO_4^-$) and subsequent electrophilic C−H activation by $HSO_4^-$. Energies relative to **INT1** for key transition states and intermediates are shown in parentheses.

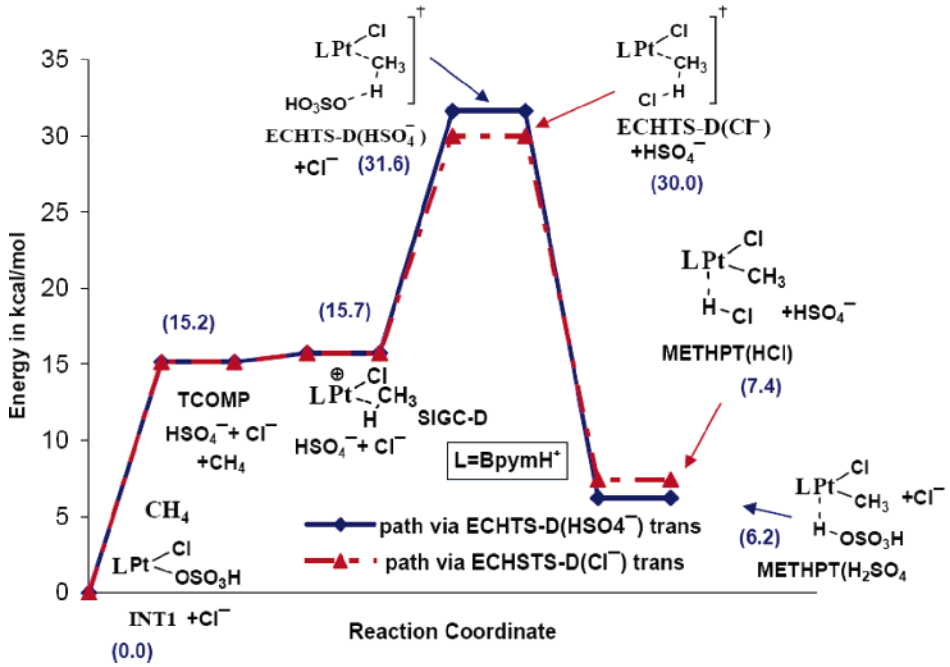


**Figure 14.** C−H activation by complex **4** through electrophilic substitution pathways: (1) dissociation of $HSO_4^-$ to form the $\sigma$-complex via **ECHTS-D**($HSO_4^-$) and subsequent electrophilic C−H activation by $HSO_4^-$, and (2) dissociation of $HSO_4^-$ to form the $\sigma$-complex via **ECHTS-D**($Cl^-$) and subsequent electrophilic C−H activation by $Cl^-$. Energies relative to INT1 for key transition states and intermediates are shown in parentheses.

This route leads to a catalytic cycle that can explain methane to methanol conversion by all Pt(II) complexes studied in this work. Alternative pathways we investigated involving interaction between $H_2SO_4$ and **METHPT**(HX) intermediates did not lead to meaningful pathways for sustaining a catalytic cycle. Furthermore, the **METHPT**(HX) intermediate of **5** does not form an adduct with $H_2SO_4$ analogous to the complex it forms with $SO_3$, and this most likely eliminates the possibility that sulfuric acid is itself acting as the oxidizing agent.

Periana suggested that the Catalytica catalyst is poisoned by the water produced during the catalytic cycle, as catalysis stops when the concentration of sulfuric acid falls below 90%.[17] This

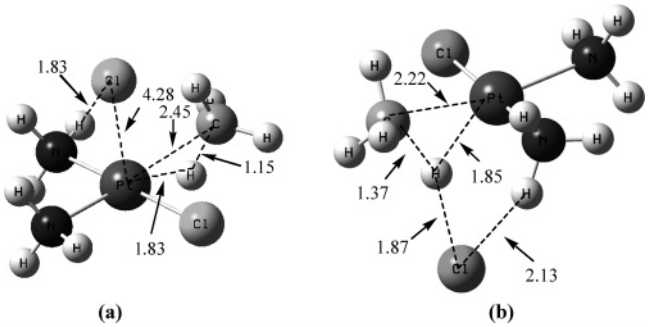


**Figure 15.** Optimized molecular structures for (a) **SIGC**($Cl^-$) and (b) **ECHTS**($Cl^-$) for complex **5**. All bond lengths are in angstroms.

can be explained if the oxidation step is inhibited by water in the reaction medium because in dilute $H_2SO_4$ it rapidly combines with $SO_3$, the anhydride of $H_2SO_4$, by a highly exothermic reaction and $H_2SO_4$ cannot itself oxidize Pt(II) to Pt(IV) in **METHPT**(HX) intermediates. Thus, the concentration of free $SO_3$ is reduced significantly in the presence of water and the production of water in the catalytic cycle poisons the catalytic process.

**METHPT**(HX) can act as a Lewis base to form adducts with Lewis acids. For instance, **METHPT** forms a Lewis acid−base adduct (**INT2**) with $SO_3$ where the $5d_{z^2}$ orbital of Pt(II) donates charge to the 3p orbital of the electrophilic S atom of $SO_3$. The adduct (Figure 18) is 4.4 kcal/mol more stable than its immediate precursors along the C−H activation by $Cl^-$ pathway for complex **1**. The Pt(II) center acts as a better Lewis base in **5** (cisplatin) (the stabilization gained from adduct formation is 10.4 kcal/mol) than it does for **1**. Formation of the Lewis acid−base adduct is followed by protonation by $H_2SO_4$ to form **INT3** (see Figure 18), which produces $HSO_4^-$ as a byproduct.

After protonation the reaction proceeds through hydroxylation of the Pt center, leading to the formation of Pt(IV). This step involves a high barrier (energy of **OXITS** relative to **INT1**) for all cases we have examined. The sensitivity of this barrier to the electronic nature of the ligands is a question of central importance in designing more effective next-generation Pt(II) complexes. Periana et al. used deuterated sulfuric acid to demonstrate that in the presence of the Catalytica complex methane undergoes deuterium exchange with $D_2SO_4$.[17] This led them to conclude that oxidation is the rate-determining step for the catalytic process. Similar experiments were not carried out for cisplatin, probably due to its fast decomposition in concentrated $H_2SO_4$.

Hydroxylation is indeed a high barrier process in the catalytic cycle involving Pt[Bpym]$Cl_2$. The hydroxylation transition state (**OXITS**) lies 44.6 kcal/mol above **INT1** for Catalytica (**1**). For the Pt(Bpym)Cl$HSO_4$ variant (**2**) the energy of **OXITS** decreases to 37.5 kcal/mol. However, the **OXITS-3a** and **OXITS-3b** energies of 46.8 and 51.8 kcal/mol are higher for protonated Catalytica (**3**), where the oxidation occurs along the catatlytic route involving C−H activation *trans* and *cis* to the protonated pyrimidine ring, respectively (see Figure 19 for optimized molecular geometries). Surprisingly, **4** (the protonated form of **2**) has a slightly lower barrier to oxidation (35.9 kcal/mol) along the catalytic route involving C−H activation *trans* to the protonated pyrimidine ring than for complex **2**. However, for complex **4**, **OXITS-3b** lies 40.8 kcal/mol above **INT1** when C−H activation occurs *cis* to the protonated pyrimidine ring. From the **OXITS** energies of complexes **1** and **2** and their corresponding protonated forms, **3** and **4**, we observe that protonation significantly affects only the relative energy of the **OXITS** transition state along the catatlytic route that proceeds via C−H activation *cis* to the protonated pyrimidine ring of the Pt(II) complexes.

For cisplatin (**5**) the relative energy of **OXITS** is 34.9 kcal/mol, significantly lower than for its Catalytica analogue (**1**), and decreases even further for $(NH_3)_2Pt(HSO_4)Cl$ (complex **6**) (28.2 kcal/mol). Thus, oxidation differentiates the relative rates of the catalytic cycle by cisplatin and Catalytica and explains the faster transformation of methane to methanol observed by Periana et al. for cisplatin.[17] The hydroxylation TS (**OXITS**) is the final TS involved in the oxidation of the Pt center. We observe that the oxidation kinetics are almost certainly determined by the electronic nature of the donor centers on the Pt(II) center. The $sp^2$-hybridized N-donors of the 2−2′ bipyrimidine (Bpym) ligand are weaker $\sigma$-electron donors than ammonia with its $sp^3$-hybridized N donor, which is less electronegative. The more electron rich Pt(II) center in cisplatin undergoes more facile oxidation than the Pt(II) center in Catalytica.

**C. Functionalization to Form $CH_3OSO_3H$.** Hydroxylation is followed by the loss of $SO_2$, which is exothermic; dissociation of **OXIP** (see Figure 20 for optimized molecular geometries) to **INT4** and $SO_2$ is favored by 11.3, 11.3, and 11.6 kcal/mol in cases of Catalytica (**1** and **2**), protonated Catalytica (**3** and **4**), and cisplatin (**5** and **6**), respectively. The five-coordinate Pt(IV) center can bond to $HSO_4^-$ from the reaction medium or undergo isomerization to the **INT5** intermediate, which has the methyl group in the axial position. **ISOMERTS** lies below the transition states for oxidation and C−H activation for all the complexes studied (31.3 kcal/mol for Catalytica). Interestingly, the isomer **INT5** is significantly more stable than **INT4** for each of the catalysts studied. **INT4** is a five-coordinate complex with $Cl^-$ in the axial position, whereas **INT5** has the methyl group in the axial position. The strong preference for the methyl group over the chloride is surprising, but may be explained by the fact that the unsaturated five-coordinate complex prefers a more polarizable $\sigma$-electron-donating group compared to the poor electron-donating chloride in the unsaturated axial position. The relative stabilities of **INT4** and **INT5** are in accordance with the rules derived for pentacoordinate complexes by Hoffmann and co-workers,[35] which suggest that for square-pyramidal complexes of $d^6$ (here, Pt(IV)) transition metals the stronger $\sigma$-donors (here $-CH_3$ group) will show a preference for the apical position.

Isomerization is followed by $S_N2$ nucleophilic attack by $HSO_4^-$ on **INT5** to form $CH_3OSO_3H$. We predict a barrier (**INT5**−**SN2TS** energy difference) corresponding to this reaction for Catalytica (**1** and **2**) of 17.9 kcal/mol. For protonated Catalytica (**3** and **4**) the barrier is 17.7 kcal/mol (see Figure 21). We predict a slightly larger barrier for the cisplatin complex (20.8 kcal/mol).

Nucleophilic displacement on Catalytica leads to the formation of the Pt(Bpym)HOCl complex, represented by the **Pt(II)-HYDROXY** intermediate in the catalytic pathway shown in Figure 1. The −OH ligand is likely to get protonated in the acidic environment to produce $H_2O$ ligated to the Pt center, but easily displaced by $H_2SO_4$ to form Pt(Bpym)Cl$(HSO_4)$, thus regenerating the active form of the catalyst, which can then initiate the next catalytic cycle. For example, protonation of the hydroxyl group of the **Pt(II)HYDROXY** intermediate formed along the catalytic cycle of complexes **3** and **4** is favorable by 12.0 kcal/mol. The barrier to displacement of $H_2O$ from the Pt center by $HSO_4^-$ is 24.7 kcal/mol, which is

(35) Rossi, A. R.; Hoffmann, R. *Inorg. Chem.* **1975**, *14*, 365.

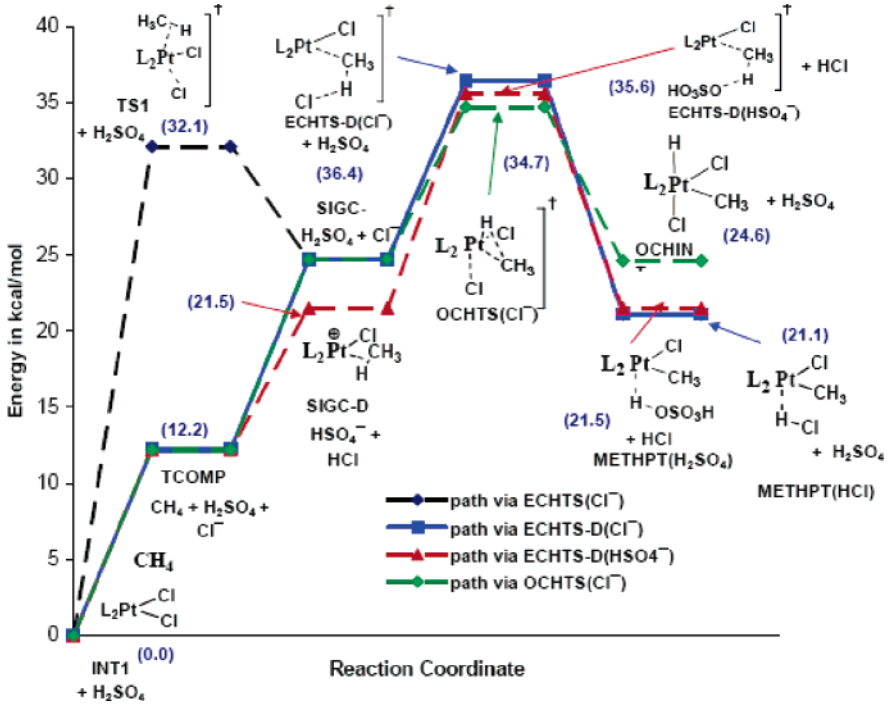


**Figure 16.** C−H activation by complex **5** through oxidative addition and electrophilic substitution pathways: (1) nucleophilic displacement to form the $\sigma$-complex via ECHTS($Cl^-$) and subsequent electrophilic C−H activation by $Cl^-$, (2) dissociation of $Cl^-$ to form the $\sigma$-complex via **ECHTS-D**($Cl^-$) and subsequent electrophilic C−H activation by $Cl^-$, (3) dissociation of $Cl^-$ to form the $\sigma$-complex via **ECHTS-D**($HSO_4^-$) and subsequent electrophilic C−H activation by $HSO_4^-$, and (4) dissociation of $Cl^-$ to form the $\sigma$-complex via **OCHTS**($Cl^-$) and subsequent oxidative C−H addition. Energies relative to **INT1** for key transition states and intermediates are shown in parentheses.

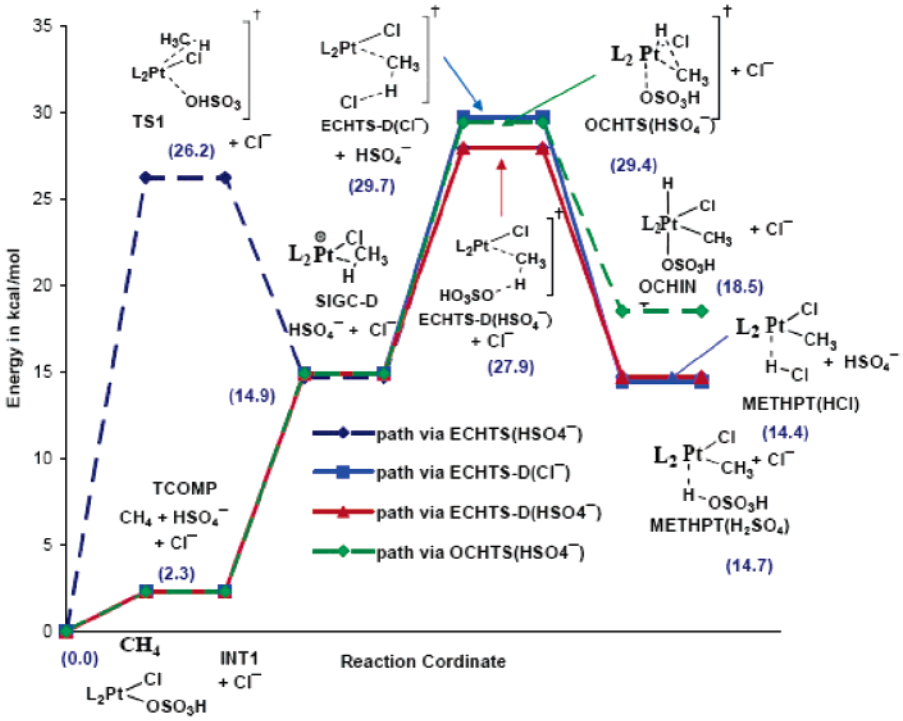


**Figure 17.** C−H activation by complex **6** through oxidative addition and electrophilic substitution pathways: (1) nucleophilic displacement to form the $\sigma$-complex via **ECHTS**($HSO_4^-$) and subsequent electrophilic C−H activation by $HSO_4^-$, (2) dissociation of $HSO_4^-$ to form the $\sigma$-complex via **ECHTS-D**($Cl^-$) and subsequent electrophilic C−H activation by $Cl^-$, (3) dissociation of $HSO_4^-$ to form the $\sigma$-complex via **ECHTS-D**($HSO_4^-$) and subsequent electrophilic C−H activation by $HSO_4^-$, and (4) dissociation of $HSO_4^-$ to form the $\sigma$-complex via **OCHTS**($HSO_4^-$) and subsequent oxidative C−H addition. Energies relative to **INT1** for key transition states and intermediates are shown in parentheses.

significantly smaller than the barrier to C−H activation and the Pt(II) to Pt(IV) oxidation barrier. Thus, active catalytic species can be easily generated. Also, the mixed aqua complex, $[Pt(BpymH)Cl(H_2O)]^{2+}$, is only 0.39 kcal/mol more stable than

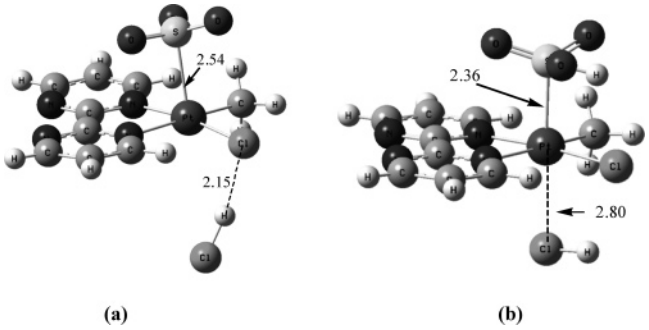


**Figure 18.** Optimized molecular geometries of (a) **INT3** and (b) **OXIINT** for complexes **1** and **2**. All bond lengths are in angstroms.

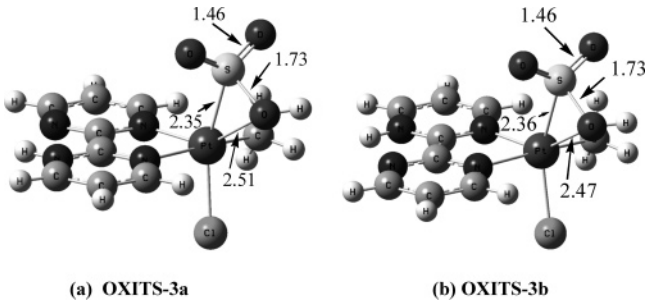


**Figure 19.** Optimized molecular geometries of **OXITS** corresponding to complexes **3** and **4** formed via C−H activation (a) *trans* and (b) *cis* to the protonated pyrimidine ring. All bond lengths are in angstroms.

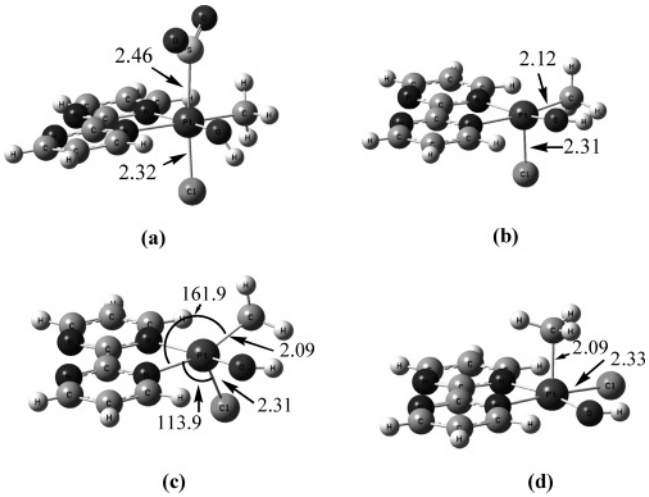


**Figure 20.** Optimized molecular geometries of (a) **OXIP**, (b) **INT4**, (c) **ISOMERTS**, and (d) **INT5** corresponding to complex **1**. All bond lengths are in angstroms and all angles are in degrees.

the mixed $HSO_4^-$ complex, $[Pt(BpymH)Cl(HSO_4)]^+$. Plots with activation barriers related to regeneration of the catalyst from the hydroxylated species are shown in the Supporting Information.

In the functionalization phase protonation of the −OH group can occur, leading to formation of a bound water molecule. This may further reduce the barrier to $S_N2$ attack, as the Pt will be rendered more electron deficient by the bound water compared to the hydroxide and hence the Pt center will serve as a better leaving group. If ligand exchange occurs between the bound water molecules and $HSO_4^-$, the $S_N2$ barrier is expected to be lower compared to the hydroxyl bound case, as $HSO_4^-$ is more electron withdrawing than −OH. The **INT5**−**SN2TS** energy difference with a $HSO_4^-$ ligand instead of a −OH bound to the

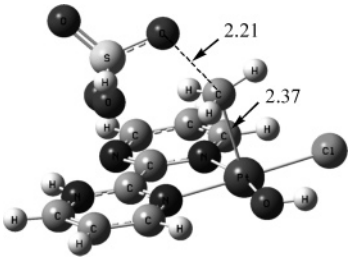


**Figure 21.** Optimized molecular geometry of **SN2TS** corresponding to complexes **3** and **4**. All bond lengths are in angstroms.

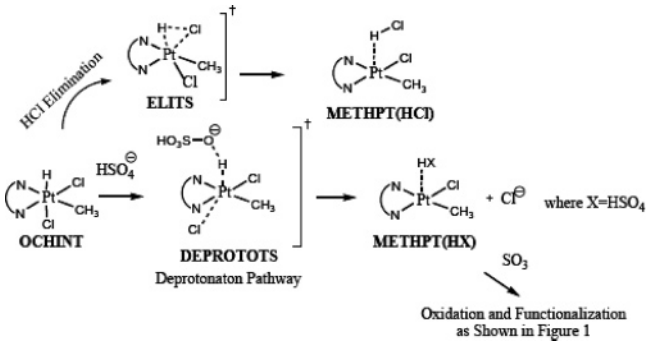


**Figure 22.** Schematic diagram of deprotonation of "C−H" oxidative addition product for complex **5** leading to subsequent pathway for catalytic transformation.

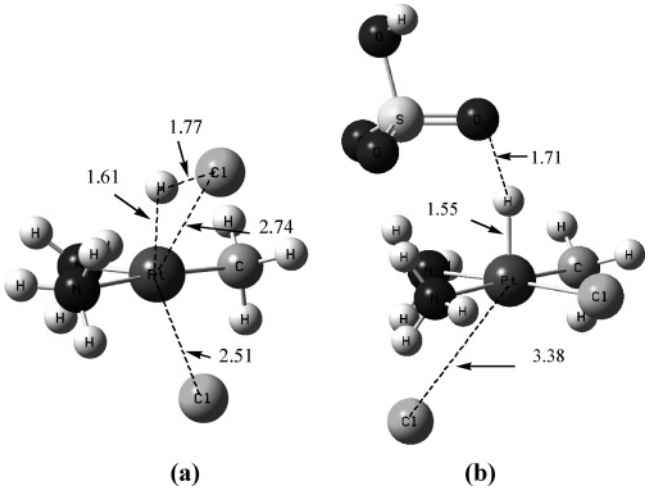


**Figure 23.** Optimized molecular geometries of (a) **ELITS** and (b) **DEPROTOTS** corresponding to complex **5**. All bond lengths are in angstroms.

Pt center has been predicted to be 10 kcal/mol by Ziegler et al. using a pure functional.[24]

**D. Does Catalysis Proceed through Oxidative C−H Addition?** We have investigated pathways to C−H functionalization via oxidative C−H addition for complex **5**. The hexacoordinate hydrido complex formed from oxidative C−H addition can undergo elimination of HCl or deprotonation (see Figure 22). HCl elimination leads to formation of the **METHPT**(HCl) intermediate, which can also be formed through the electrophilic C−H activation route. The barrier to HCl elimination from **OCHINT** is relatively large, as the transition state for HCl elimination lies 33.0 kcal/mol above **OCHINT** and 51.0 kcal/mol above **INT1**, practically eliminating the prospect of catalysis through this route. Another possibility is deprotonation and simultaneous detachment of $X^-$ to form **METHPT**($H_2SO_4$). The energetic cost of deprotonation is not prohibitive. The transition state to deprotonation

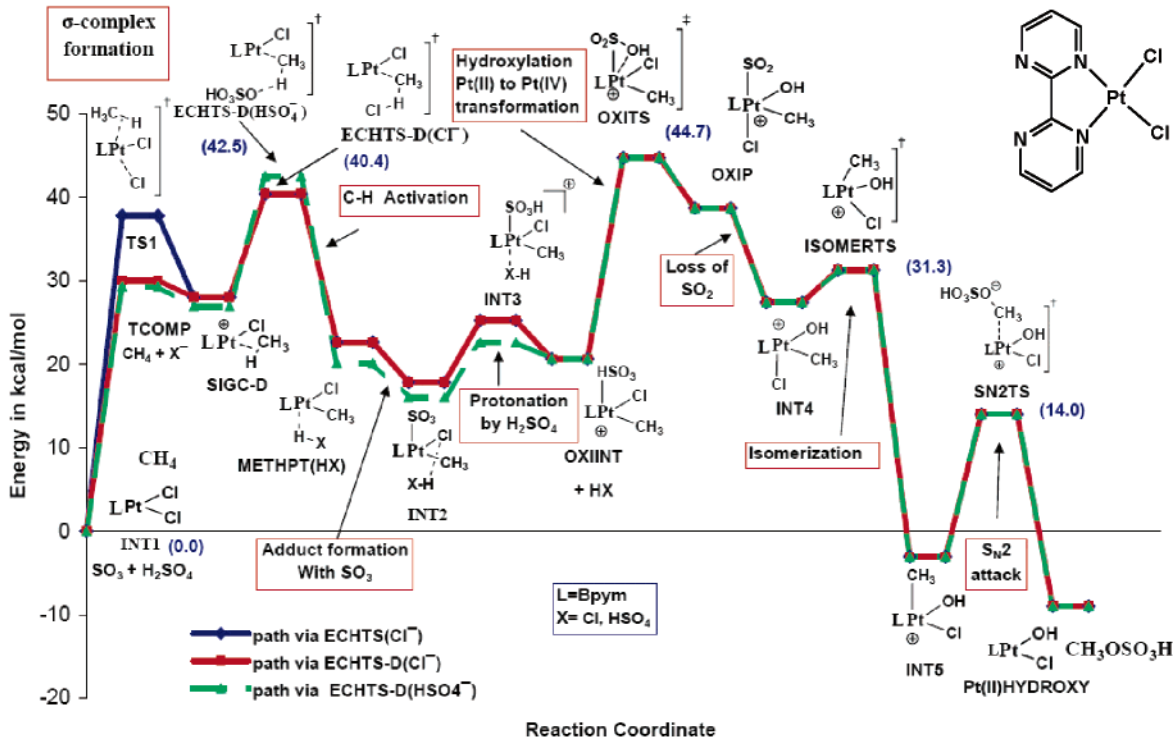


**Figure 24.** Schematic potential energy profile for the catalytic cycle of complex **1** in $H_2SO_4$ through electrophilic C−H activation channels.

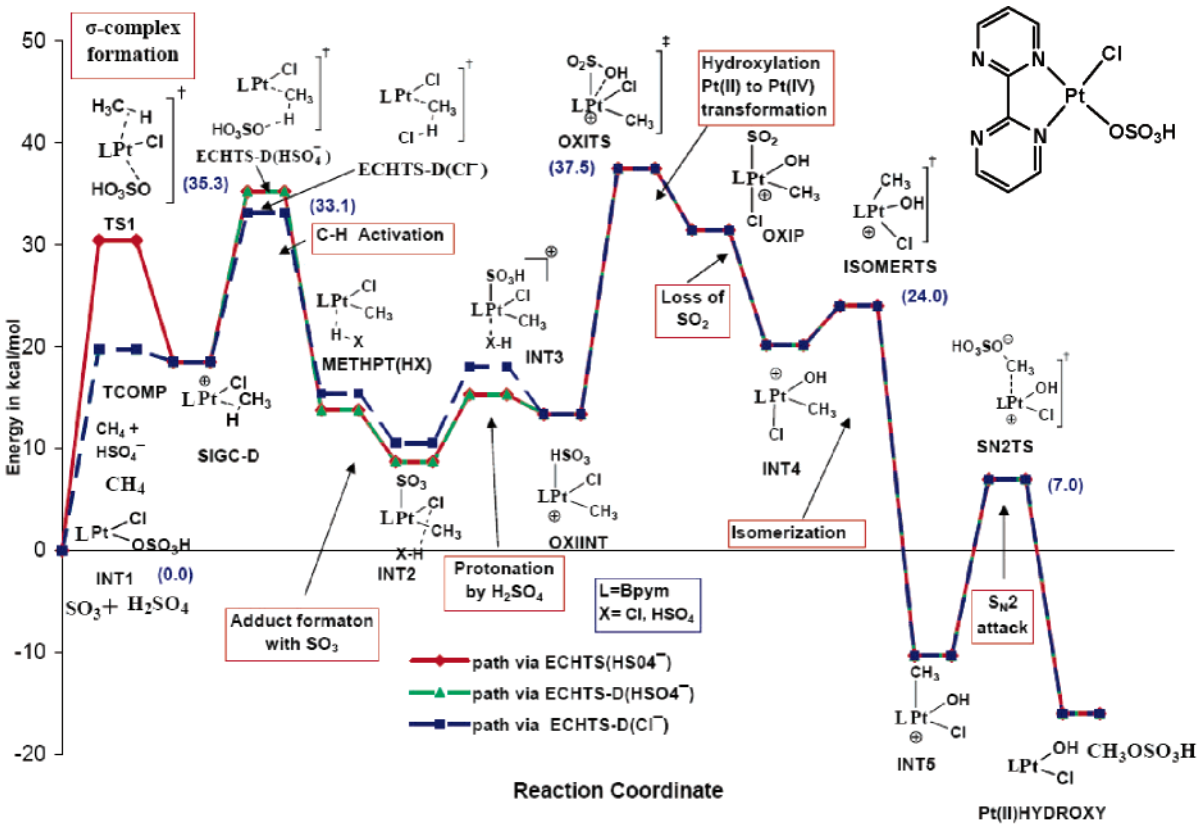


**Figure 25.** Schematic potential energy profile for the catalytic cycle of complex **2** in $H_2SO_4$ through electrophilic C−H activation channels.

(**DEPROTOTS**) (see Figure 23) lies 31.4 kcal/mol above **INT1**. Deprotonation is then followed by the catalytic route discussed above (Figure 1). The full potential energy profile is discussed in the following section.

**E. Full Potential Energy Profiles of Pt(II) Complexes.** The main objectives of this work are to determine the relative energies of intermediates and transition states for the catalytic cycles of the four likely active forms of the Catalytica complex in concentrated $H_2SO_4$, to plot their full potential energy profiles, and thus identify the active mechanism of methane to methanol conversion. In plotting the full potential energy profiles, we have integrated the three major phases of the catalytic cycle for each complex studied. Although we have calculated that electrophilic C−H activation can proceed by several routes, we illustrate only

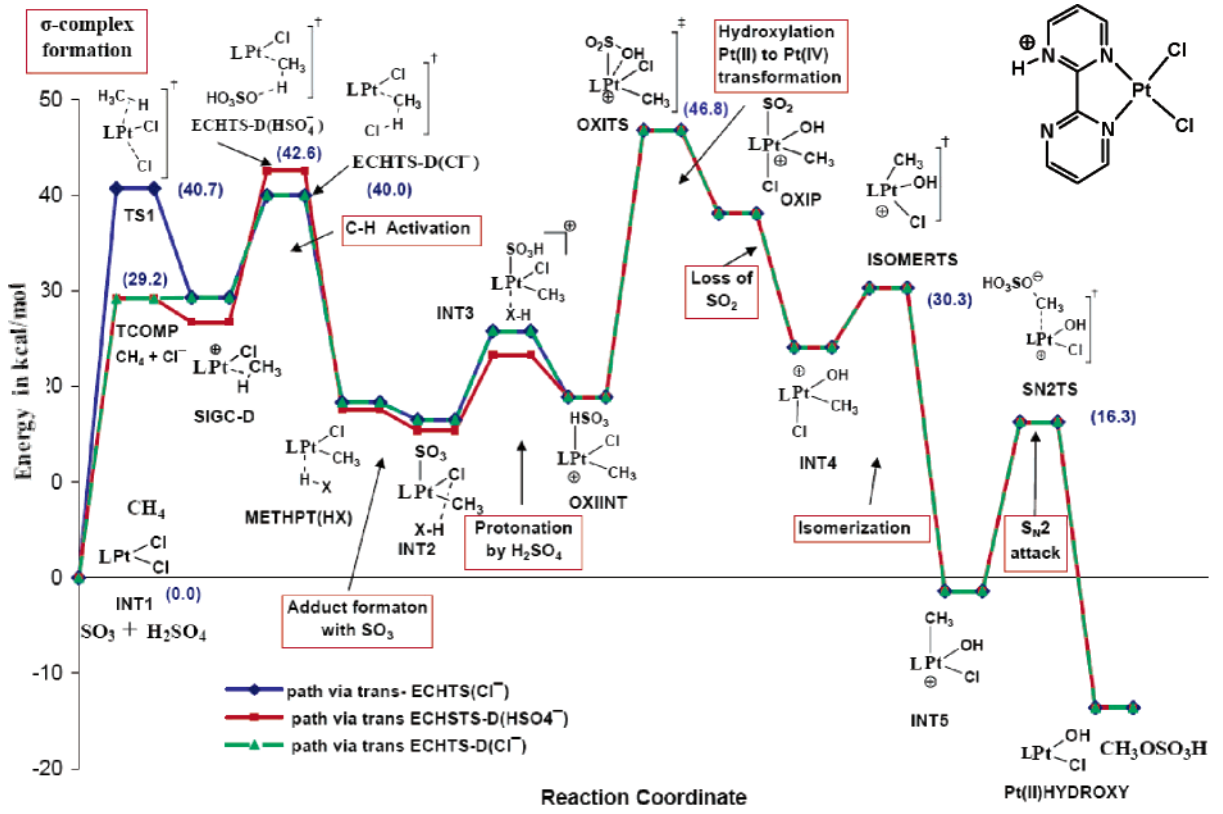


**Figure 26.** Schematic potential energy profile for the catalytic cycle of complex **3** in $H_2SO_4$ through electrophilic C−H activation channels.

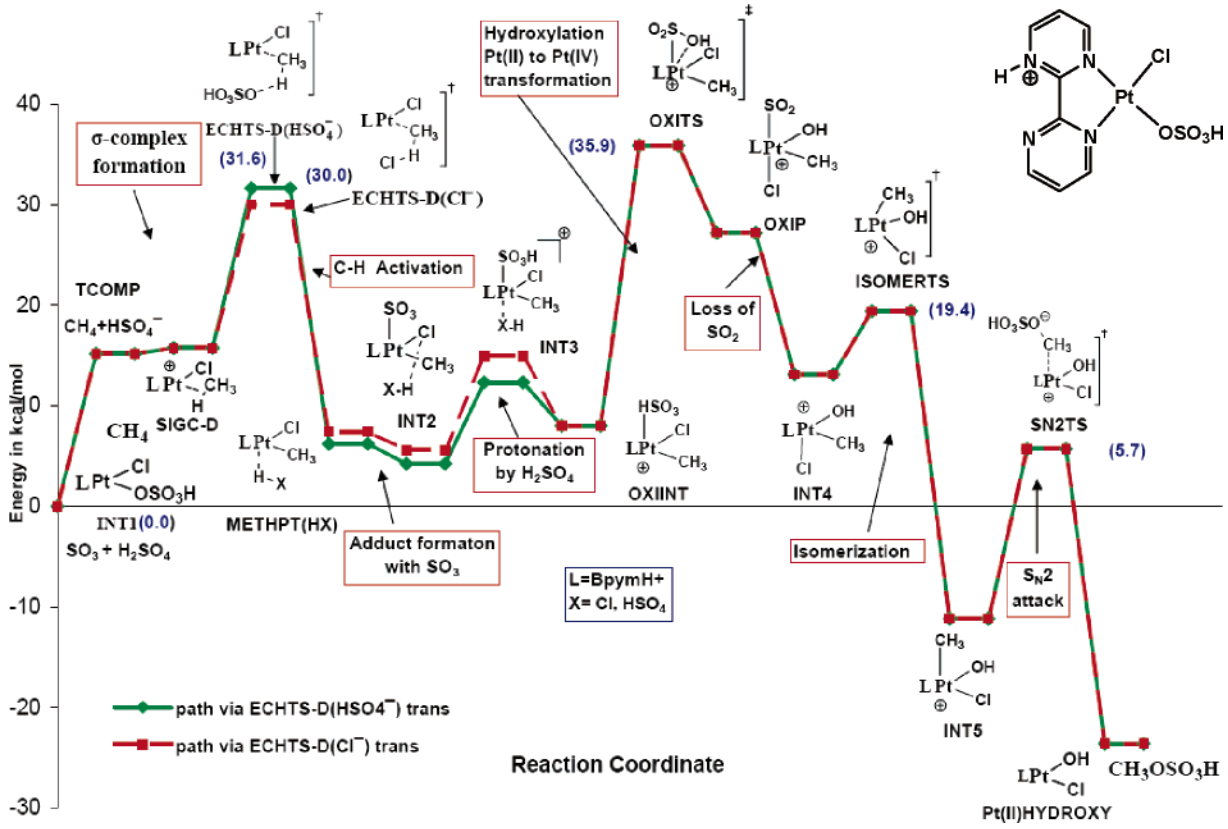


**Figure 27.** Schematic potential energy profile for the catalytic cycle of complex **4** in $H_2SO_4$ through electrophilic C−H activation channels.

the most probable routes considering both barrier heights and concentrations of key anions that may be involved in the reaction. In certain cases additional low-barrier, but less probable routes are also depicted in Figures 24−30.

A comparison of the three profiles strongly indicates that the rate of catalysis by the Pt(II) complexes are determined by oxidation and C−H activation. We observe that these two bottlenecks are smallest for $[Pt(BpymH)ClHSO_4]^+$ (**4**). The

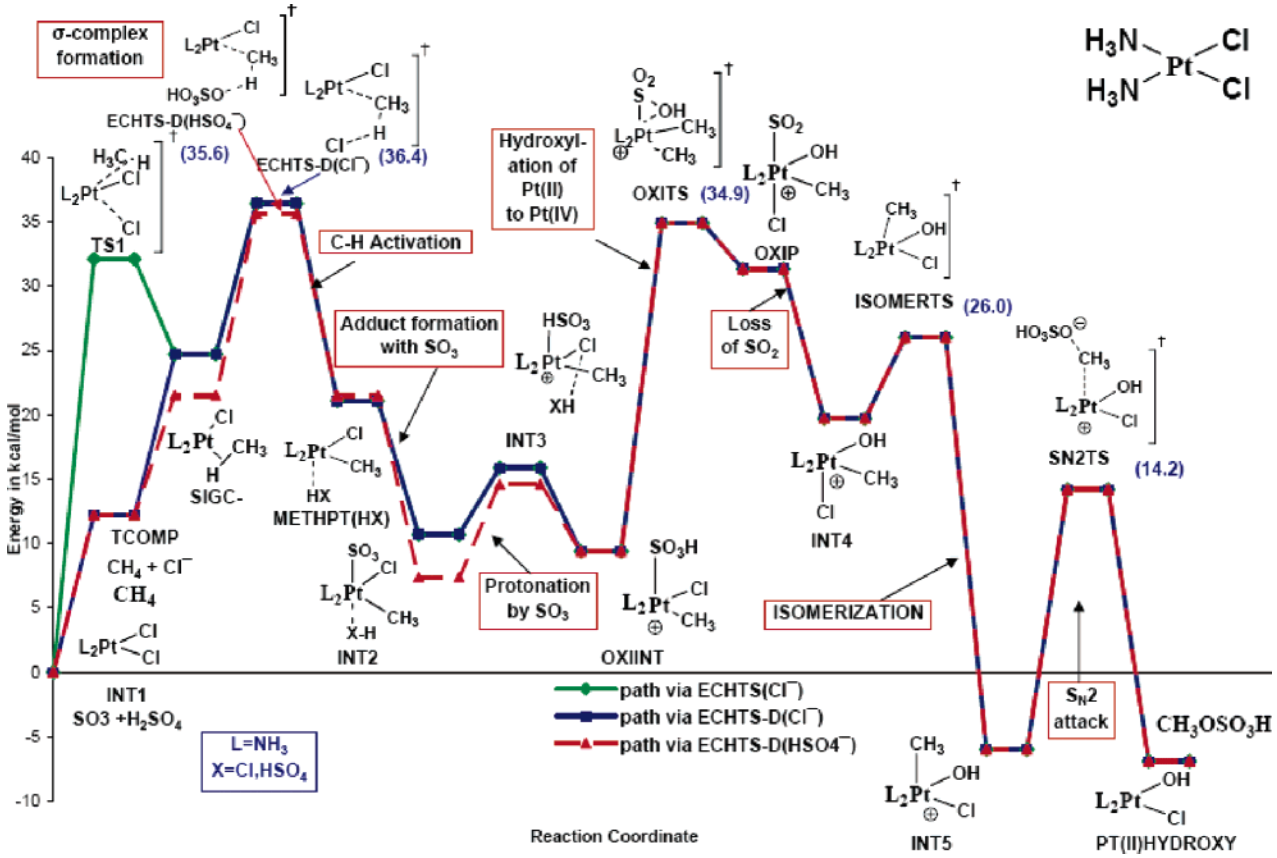


**Figure 28.** Schematic potential energy profile for the catalytic cycle of complex **5** in $H_2SO_4$ through electrophilic C−H activation channels.

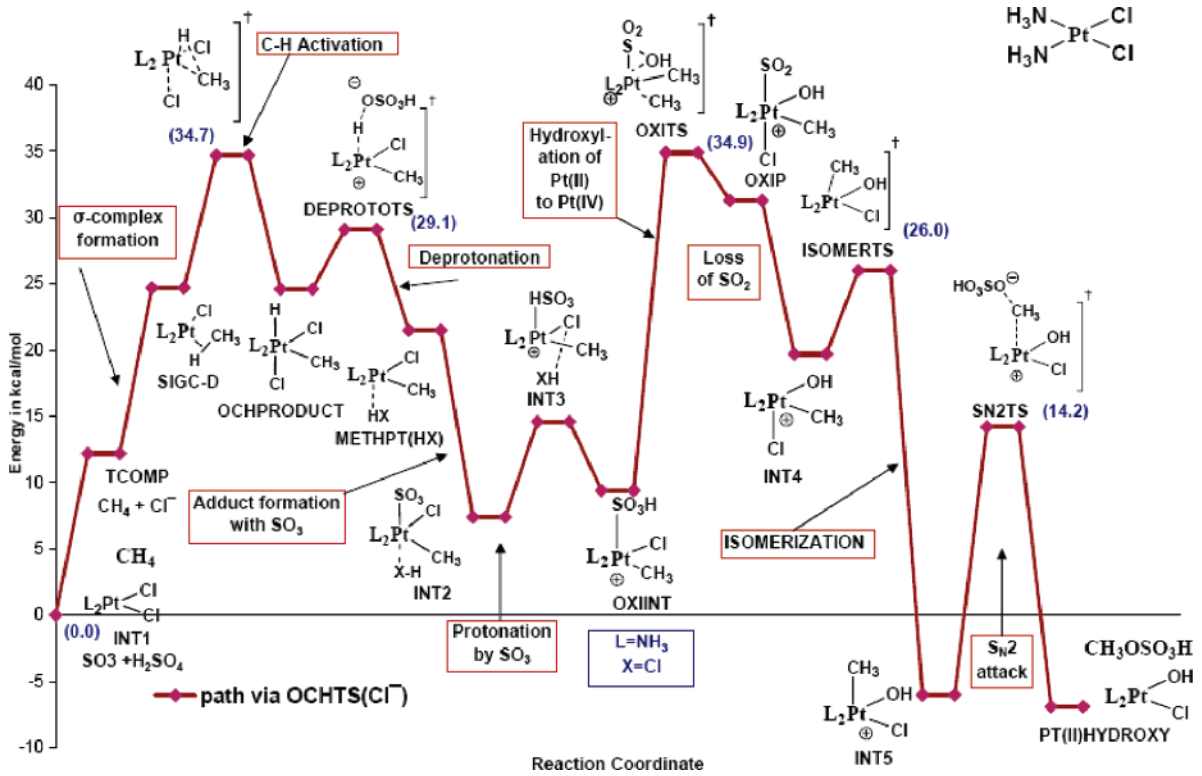


**Figure 29.** Schematic potential energy profile for the catalytic cycle of complex **5** in $H_2SO_4$ through oxidative C−H addition channels.

activation barrier associated with the hydroxylation step is highest in energy (35.9 kcal/mol above **INT1**). C−H activation is the other significant barrier, with the **ECHTS-D**($HSO_4^-$) 31.6 kcal/mol above **INT1**, 4.3 kcal/mol smaller than the highest barrier encountered in the oxidation phase. The C−H activation barrier is even smaller (30.0 kcal/mol) if free $Cl^-$ carries out C−H activation in the catalytic route of **4**. It is improbable that complex **3**, although protonated, is the active catalyst form, as the barrier to oxidation is prohibitively large (46.8 kcal/mol).

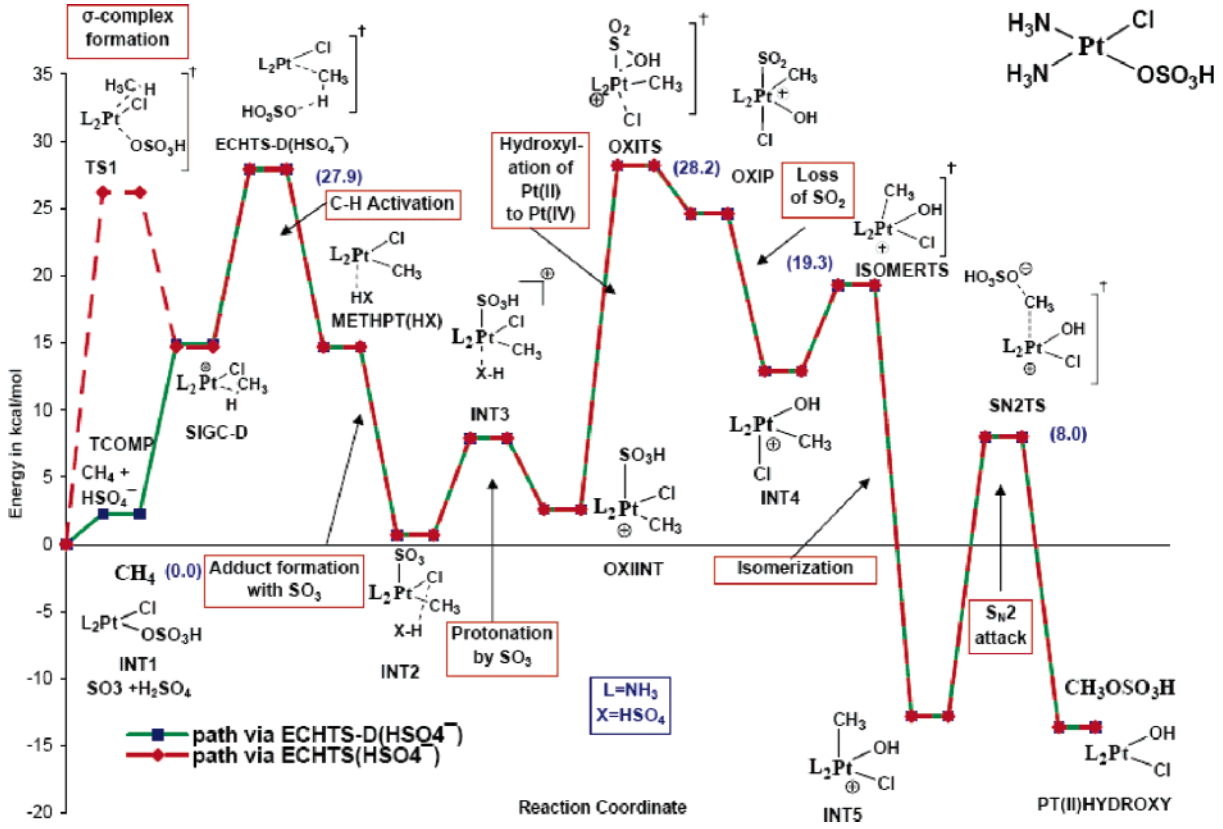


**Figure 30.** Schematic potential energy profile for the catalytic cycle of complex **6** in $H_2SO_4$ through electrophilic C−H activation channels.

We find that protonation of the Bpym backbone does not necessarily have any significant detrimental effect on the lowest lying catalytic routes. As discussed earlier, it significantly affects only the reaction barriers for the catalytic route via C−H activation *cis* to the protonated pyrimidine ring. It was previously suggested that protonation of the Bpym ring significantly affects the oxidation process on the basis of DFT thermodynamic calculations. However, it was not clearly indicated whether they considered oxidation of the C−H activated product *cis* or *trans* with respect to the protonated pyrimidine ring.[25]

Our results substantiate the experimental observation of deuterium exchange in the deuteriated solvent with methane at 150 °C without the production of $CH_3OSO_3H$. The differences of 4.2−5.9 kcal/mol (see Figure 27) between the oxidation barrier and C−H activation barrier for complex **4** suggests that at lower temperatures Pt(II) to Pt(IV) oxidation can be substantially suppressed while C−H activation leading to deuterium exchange remains active. This is the first theoretical demonstration of Periana et al.'s deuterium exchange results.[17] The difference between these barriers can be further examined using other DFT functionals, solvent models, and full optimization within a solvent model, but this is beyond the scope of the current work.

For **5** we predict that the lowest barrier route for $CH_4$ to $CH_3OSO_3H$ is the oxidative C−H addition pathway, with a barrier 1.7 kcal/mol lower than that of electrophilic C−H substitution (see Figures 28 and 29 for potential energy profiles). Note that for complex **5** we observe that Pt(II) to Pt(IV) oxidation is slightly favored over electrophilic C−H activation by 1.5 kcal/mol. Although we find that the catalytic route via oxidative C−H addition is slightly more favorable than the electrophilic C−H activation route, the energy differences are small relative to both the resolution of the methods we employ and considering the branching ratios such a difference produces at the temperatures at which the reactions are carried out.

A comparison between the catalytic profiles of **5** and **6** indicates that the barriers associated with $(NH_3)_2PtClHSO_4$ (**6**) are the lowest of all the catalyst species considered (see Figures 28, 29, and 30). This is due to the smaller barrier to oxidation, as **OXITS** lies only 28.2 kcal/mol above **INT1** for $(NH_3)_2$-$PtClHSO_4$. Furthermore C−H activation remains a lower barrier process than oxidation, with a barrier of 27.9 kcal/mol for **6**. The lower barrier to oxidation for complex **6** than those of complexes **1**, **2**, **3**, and **4** explains the faster conversion of methane to methanol by cisplatin compared to Catalytica. Although our calculations clearly indicate that the barriers associated with N-$sp^3$ donor ligands are considerably smaller than those associated with N-$sp^2$ ligands, they are not potential targets as catalysts because $NH_3$-based Pt complexes easily decompose in the highly acidic $H_2SO_4$ medium. This problem can be avoided by combining two strategies: (i) using a bidentate N-$sp^3$-based ligand and (b) providing additional protonation sites remote to the N-$sp^3$ donor centers, for example on a side chain of the bidentate ligands, so that they have little effect on the N-$sp^3$ donors upon protonation in $H_2SO_4$. The first strategy ensures stability of the complex due to entropic factors, and the second strategy ensures stability from enthalpic factors, as the protonation on the side chain makes the ligand less susceptible to further protonation, as has been suggested for Catalytica by Goddard et al. Investigation of certain prototypes of these ligands is in progress and will be reported in a future publication. The other potentially viable strategy is to add electron-donating groups to the Bpym ligand to decrease the barrier to oxidation.

## Conclusions

This theoretical study establishes the full potential energy profiles for the catalytic cycles of methane to methanol

conversion by Catalytica and cisplatin and explains the faster rate of catalysis for cisplatin compared to Catalytica based on computed barriers for Pt(II) to Pt(IV) oxidation. Our calculations also reveal that the oxidation of Pt(II) to Pt(IV) is rate limiting for protonated Catalytica forms. However, C−H activation also involves a significantly high barrier. The energy of the oxidation transition state (**OXITS**) is significantly affected by the nature of the ligands. N-$sp^3$ donors make Pt(II) to Pt(IV) oxidation facile compared to Bpym, a $\sigma$-donor $\pi$-acid ligand. However, protonation of the Bpym ligand of Catalytica does not siginificantly affect the barrier to Pt(II) to Pt(IV) oxidation if it proceeds through "C−H activation" *trans* to the pyrimidine ring. Moreover, our results provide a theoretical description of the isotopic exchanges observed by Periana et al. Additionally, we have established a route for methane to methanol conversion operating via oxidative C−H addition and subsequent deprotonation for cisplatin. Our calculations suggest the catalytic transformation occurs favorably through oxidative C−H addition and also through electrophilic C−H activation for cisplatin.

**Acknowledgment.** The authors would like to thank the Pittsburgh Supercomputing Center for providing computational time for this project. A.P. would also like to thank Lars Nielsen for help in editing the manuscript.

**Supporting Information Available:** The optimized Cartesian coordinates of all the intermediates and transition states, potential energy profiles for regeneration of active catalyst form, free energies of activation of key steps, balanced chemical equations used for plotting the potential energy profiles, and gas and solution phase total energies are provided. This material is available free of charge via the Internet at http://pubs.acs.org.

OM060465J